



# Immunoproteasome Activation Expands the MHC Class I Immunopeptidome, Unmasks Neoantigens, and Enhances T-cell Anti-Myeloma Activity

Priyanka S. Rana<sup>1,2</sup>, James J. Ignatz-Hoover<sup>1,2</sup>, Chunna Guo<sup>3,4</sup>, Amber L. Mosley<sup>3,4</sup>, Ehsan Malek<sup>1,2,5</sup>, Yuriy Federov<sup>6</sup>, Drew J. Adams<sup>6</sup>, and James J. Driscoll<sup>1,2,5</sup>

## ABSTRACT

Proteasomes generate antigenic peptides that are presented on the tumor surface to cytotoxic T-lymphocytes. Immunoproteasomes are highly specialized proteasome variants that are expressed at higher levels in antigen-presenting cells and contain replacements of the three constitutive proteasome catalytic subunits to generate peptides with a hydrophobic C-terminus that fit within the groove of MHC class I (MHC-I) molecules. A hallmark of cancer is the ability to evade immunosurveillance by disrupting the antigen presentation machinery and down-regulating MHC-I antigen presentation. High-throughput screening was performed to identify compound A, a novel molecule that selectively increased immunoproteasome activity and expanded the number and diversity of MHC-I-bound peptides presented on multiple myeloma cells. Compound A increased the presentation of individual MHC-I-bound peptides by >100-fold and unmasked tumor-specific neoantigens on myeloma cells. Global proteomic integral stability assays determined that

compound A binds to the proteasome structural subunit PSMA1 and promotes association of the proteasome activator PA28 $\alpha/\beta$  (PSME1/PSME2) with immunoproteasomes. CRISPR/Cas9 silencing of *PSMA1*, *PSME1*, or *PSME2* as well as treatment with immunoproteasome-specific suicide inhibitors abolished the effects of compound A on antigen presentation. Treatment of multiple myeloma cell lines and patient bone marrow-derived CD138<sup>+</sup> cells with compound A increased the anti-myeloma activity of allogeneic and autologous T cells. Compound A was well-tolerated *in vivo* and co-treatment with allogeneic T cells reduced the growth of myeloma xenotransplants in NOD/SCID gamma mice. Taken together, our results demonstrate the paradigm shifting impact of immunoproteasome activators to diversify the antigenic landscape, expand the immunopeptidome, potentiate T-cell-directed therapy, and reveal actionable neoantigens for personalized T-cell immunotherapy.

## Introduction

The transformative success of immunotherapy to activate the immune system and induce long-lasting responses has revolutionized cancer treatment (1). However, only a fraction of patients respond to immunotherapy, and cancer cells escape the antigen presentation machinery (APM) and immunosurveillance through molecular mechanisms that remain elusive (2). Proteasomes play a central role in the immune response by generating peptides from intracellular antigens that are presented on the cell surface for recognition by CD8<sup>+</sup> cytotoxic T-lymphocytes (CTL;

ref. 3). Immune cells contain highly specialized proteasomal variants, immunoproteasomes, that are specially adapted for a role in MHC class I (MHC-I) antigen presentation to CTLs (4, 5). To process antigens more efficiently, the three constitutive proteasome catalytic subunits ( $\beta$ 1,  $\beta$ 2, and  $\beta$ 5) are replaced with specialized catalytic subunits ( $\beta$ 1i,  $\beta$ 2i, and  $\beta$ 5i), which are co-operatively incorporated to form immunoproteasomes (6, 7). These findings suggest that a highly sophisticated proteolytic machinery with functional plasticity is required to generate finely tailored products.

Emerging therapies, such as immune checkpoint blockade, T-cell receptor (TCR)-engineered T cells, and adoptive T-cell transfer, have focused attention on the presentation of cancer-associated antigens that are targeted by engineered T-cell therapy (8, 9). Although the mechanisms of action behind these therapies vary tremendously, their core component is the ability to induce T cells to target cancer cells after TCR recognition of the appropriate antigenic peptides complexed with MHC-I molecules (10). However, low-density surface presentation of tumor-associated antigens (TAAg), lack of immunogenic neoantigens (NeoAg), and the ability of cancer cells to downregulate the APM hinder the ability of T cells to eliminate cancer cells (11–13). Studies performed in lung, melanoma, bladder, and colorectal carcinomas have shown that up to two-thirds of tissue samples and cell lines harbor alterations in the APM including loss of the human leukocyte antigen (HLA) class I locus and  $\beta$ 2-microglobulin mutations (14–17). Immunoproteasome expression is associated with better prognosis and response to checkpoint therapies, whereas immunoproteasome deficiency is a feature of non-small cell lung cancer and associated with poor outcome (18–21).

<sup>1</sup>Case Comprehensive Cancer Center, School of Medicine, Case Western Reserve University, Cleveland, Ohio. <sup>2</sup>Division of Hematology and Oncology, Department of Medicine, Case Western Reserve University, Cleveland, Ohio. <sup>3</sup>Center for Proteome Analysis, Indiana University School of Medicine, Indianapolis, Indiana. <sup>4</sup>Department of Biochemistry and Molecular Biology, Indiana University School of Medicine, Indianapolis, Indiana. <sup>5</sup>Adult Hematologic Malignancies and Stem Cell Transplant Section, Seidman Cancer Center, University Hospitals Cleveland Medical Center, Cleveland, Ohio. <sup>6</sup>Small Molecule Drug Discovery Core, Case Western Reserve University, Cleveland, Ohio.

**Corresponding Author:** James J. Driscoll, Internal Medicine/HemeOnc, University Hospitals Cleveland Medical Center, 2103 Cornell Road, WRB 2-126, Cleveland, OH 44106. E-mail: James.Driscoll@UHhospitals.org

Mol Cancer Ther 2024;23:1743–60

doi: 10.1158/1535-7163.MCT-23-0931

This open access article is distributed under the Creative Commons Attribution-NonCommercial-NoDerivatives 4.0 International (CC BY-NC-ND 4.0) license.

©2024 The Authors; Published by the American Association for Cancer Research

We hypothesized that the selective activation of immunoproteasomes would increase the abundance and diversity of the MHC-I immunopeptidome to enhance CTL antitumor activity. Here, high-throughput screens identified an immunoproteasome-selective activator (compound A) that increased antigen presentation in murine and multiple myeloma cells. Mass spectrometry (MS) revealed that compound A enhanced the abundance of MHC-I-bound TAAgs and NeoAgs to expand and amplify immunopeptidome diversity. Compound A also significantly promoted the cytotoxic power of autologous patient CTLs.

## Materials and Methods

### Cell lines

The multiple myeloma cell lines (MMCL) RPMI-8226, ARH-77, U266, and MM1.S were authenticated and provided by ATCC. Cells were cultured in complete RPMI-1640 medium supplemented with 1% penicillin/streptomycin and 10% FBS according to the manufacturer's guidelines. Mouse lymphoblast cell line E.G7-Ova (ATCC) was generated by incorporation of a plasmid expressing chicken ovalbumin (*Ova*) into EL4 cells. E.G7-Ova cells were cultured in RPMI-1640 medium supplemented with 0.05 mmol/L  $\beta$ -mercaptoethanol, 0.4 mg/mL G418, 1% penicillin/streptomycin, and 10% FBS. The B3Z CD8<sup>+</sup> T-cell hybridoma, specific for the SIINFEKL (OVA<sub>257-264</sub>/K<sup>b</sup>) peptide, was a kind gift from Dr. J.D. Sauer (University of Wisconsin-Madison). B3Z cells were cultured in R10 media that contained 500  $\mu$ g/mL G418 (Geneticin). HeLa cells (ATCC) were cultured in complete DMEM supplemented with 10% FBS. Cell lines were cultured at 37°C in a humidified incubator supplemented with 5% CO<sub>2</sub> and were periodically tested for mycoplasma. Human embryonic kidney (HEK)293T cells were obtained from ATCC and cultured according to the manufacturer's guidelines. Cell lines were authenticated and tested for mycoplasma contamination by ATCC.

### Reagents

Proteasome inhibitors bortezomib, ONX-0912, and ONX-0914 were obtained from SelleckChem. Histone deacetylase (HDAC)-targeted library is a highly curated collection of small molecule compounds specifically targeted at HDACs as a powerful tool for drug discovery (ChemDiv). The HDAC-targeted library contains 9,760 screening compounds that undergo thorough quality control assessments using LC/MS and/or <sup>1</sup>H NMR to guarantee a purity threshold of >90%. The structures of compounds A through H are shown in Supplementary Fig. S1 and are based on information provided by ChemDiv. For subsequent studies, additional quantities of compounds A through H were synthesized by ChemDiv as indicated in Supplementary Fig. S2 and ref. 22. The novel structures of compounds A through H, the step-by-step synthesis details, and product characterization data are included in Supplementary Figs. S1 and S2. ChemDiv custom synthesis products are subjected to quality control by NMR and LC/MS, and purity is guaranteed to be >90%. Tubastatin A (S2627, CAS:1310693-92-5, batch O3, 97.42% purity), ACY-738 (S8648, CAS: 1375465-91-0, batch S864802, 99.80% purity), ACY-1215 (S8001, CAS: 1316214-4, batch 04, HPLC purity 99.26%), and nexturastat A (S7473, CAS:1403783-31-2; batch 01, 99.65% purity) were obtained from SelleckChem. Methods of synthesis for tubastatin A, ACY-738, ACY-1215, and nexturastat A have been previously described (23–26). KZR-616 was obtained from MedChemExpress. The immune checkpoint inhibitors (ICI) pembrolizumab, nivolumab, durvalumab, and atezolizumab were

obtained from SelleckChem. Fluorogenic peptide substrates were from Sigma, Cayman Chemicals, Millipore, and Boston Biochem. General chemicals, reagents, and buffers were from Thermo Fisher Scientific.

### High-throughput screens

RPMI-8226 cells were seeded in 384-well, black-walled, clear bottom plates (30,000 cells/well) and incubated with compounds (10  $\mu$ mol/L) for 18 hours. The cell-permeable proteasome-specific substrate LLVY-R110 was added and incubation continued for 21 hours at 37°C. Fluorescence intensity was measured at  $\lambda$ EX 490 nm and  $\lambda$ EM 525 nm to monitor the effect of the compounds on activity. The ChemDiv HDAC-targeted library was screened using the RPMI-8226 cells and described assay. Compounds that increased proteasome activity by  $\geq$ 50% and maintained cell viability in  $\geq$ 90% of controls treated with 0.05% DMSO were deemed hits.

### Measurement of proteasome and immunoproteasome peptide-hydrolyzing activity

The cell permeable substrate LLVY-R110 (Sigma MAK-172A) was used to measure proteasomal chymotrypsin (ChT)-like peptide-hydrolyzing activity in multiple myeloma cells. Cells (30,000/well) were seeded into 96-well, black-walled clear bottom plates in a final volume of 100  $\mu$ L/well. Cells were treated with vehicle (0.05% DMSO) or compounds at the given concentrations for indicated times. Following incubation, proteasome substrate LLVY-R110 (Sigma, MAK-172B) reconstituted in assay buffer was added and plates were incubated at 37°C for 21 hours protected from light. Fluorescence intensity as a measure of LLVY-R110 cleavage was monitored at  $\lambda$ EX 490 nm and  $\lambda$ EM 525 nm. To measure proteasome activity in cell lysates, the fluorogenic peptide substrates LLVY-R110 (25  $\mu$ mol/L), Ac-ANW-AMC (15  $\mu$ mol/L; Cayman Chemicals, 26640), Suc-LLVY-AMC (100  $\mu$ mol/L; Sigma, S6510), Z-LLL-AMC (100  $\mu$ mol/L; Cayman Chemicals, 10008118), Ac-WLA-AMC (30  $\mu$ mol/L; Boston Biochem, S-330), Boc-LRR-AMC (30  $\mu$ mol/L; Cayman chemicals, 26642), Ac-RLR-AMC (30  $\mu$ mol/L; Cayman chemicals, 26643), Z-ARR-AMC (30  $\mu$ mol/L; MilliporeSigma 5391-49), Z-LLE-AMC (30  $\mu$ mol/L; Cayman chemicals, #10008117), and ANC-PAL-AMC (30  $\mu$ mol/L; Boston Biochem, S-310) were used. Cells were treated with vehicle or compound A for 48 hours after which they were washed with PBS, pelleted, and lysed in assay buffer that contained 50 mmol/L HEPES (Acros, 17257), 10 mmol/L NaCl (Sigma, S5150), 1.5 mmol/L MgCl<sub>2</sub> (Alfa Aesar, J62411), 1 mmol/L EDTA (Millipore, 324504), 1 mmol/L EGTA (BioWorld, 40120128-1), 250 mmol/L sucrose (Sigma-Aldrich, S9378), 5 mmol/L dithiothreitol (DTT; Life Technologies, 15508013), and 2 mmol/L ATP (Sigma, A3377). Lysate was sonicated for 10 seconds using a microtip, centrifuged at 16,000  $\times$  g for 10 minutes, and the supernatant used for assays. Cell lysate (50  $\mu$ L/assay) was added to 96-well black-walled plates (Corning) followed by substrate addition and incubation for 3 hours at 37°C. Fluorescence intensity was measured at the respective excitation and emission spectrum for each fluorogenic peptide using a SpectraMax i3 plate reader interfaced with SoftMax Pro Software Validation Package (Molecular Devices).

### Proteome integral solubility alteration

RPMI-8226 cells ( $1 \times 10^7$ ) were treated with compound A (1  $\mu$ mol/L) for 6 and 24 hours in triplicate. Proteome integral solubility alteration (PISA) lysis buffer (40 mmol/L HEPES pH 7.5, 200 mmol/L NaCl, 5 mmol/L  $\beta$ -glycerophosphate, 0.1 mmol/L sodium orthovanadate, 2 mmol/L tris (2-carboxy-ethyl)-phosphin-

HCl, 0.4% NP40, and Roche EDTA-free protease inhibitor) was added. Cells were subjected to lysis in a Diagenode Bioruptor, and equal aliquots of PISA lysates were subjected to gradient heat treatment in a thermocycler. Heat-treated and unheated (global) samples were processed with reduction, alkylation, and digested with LysC/trypsin in 8 mol/L urea in 100 mmol/L Tris-HCl, pH 8.0, according to the manufacturer's (Promega) protocols. Digested samples were labeled with TMTpro (Thermo Fisher Scientific, Lot# YD368822). After labeling, QC runs were performed on a QE Plus mass spectrometer to check labeling efficiency. Tandem mass tags (TMT)-labeled samples were pooled, and high-pH reversed-phase peptide fractionation was performed to obtain eight biochemical fractions analyzed on an Orbitrap Eclipse (Thermo Fisher Scientific). The mass spectrometer was operated using a custom data-dependent method, with MS performed in the Orbitrap at 120,000 full-width-half-maximum (FWHM) resolution and sequential MS-MS performed using a resolution of 50,000 FWHM and higher energy, collision-induced dissociation. MS-MS data were acquired with a first mass set at 100 m/z to capture TMTPro reporter ions. A 4-second cycle time was employed for all steps with a segmented acquisition using high-field asymmetric waveform ion mobility spectrometry voltages of  $-45$  V,  $-55$  V, and  $-65$  V (for 1.3 seconds each). Protein identification and quantification were performed using Proteome Discoverer 2.5 (Thermo Fisher Scientific) against a human proteome database (FASTA obtained from UniProt). Carbamidomethyl (+57.021Da) and TMTpro labeled on lysine (K) and peptide N-termini were set as static modifications. Percolator FDR cutoff was set at 1%. Median normalization and treatment to vehicle ratio were performed to identify target proteins of compound A. Two-tailed student *t* test (with equal or unequal variance depending on *F* test) was applied to calculate *P* values within Proteome Discoverer.

### Measurement of cell viability

Cells (300,000/well in 100  $\mu$ L) were suspended in complete RPMI media that lacked phenol red and seeded in 96-well plates. Following treatment, viability was determined using the 2,3-bis[2-methoxy-4-nitro-*S*-sulfophenyl]-2H-tetrazolium-5-carboxanilide inner salt assay (27). Cells were labeled with 4 mg/mL 2,3-bis-(2-methoxy-4-nitro-5-sulfophenyl)-2H-tetrazolium-5-carboxanilide (Gold Biotechnology, X-200-100) dissolved in PBS containing phenazine methosulfate (Sigma) and incubated at 37°C. Absorbance was measured at 450 nm using a SpectraMax i3 plate reader.

### Flow cytometry

Cells were washed with PBS and stained with the indicated cell surface markers in FACS buffer (PBS, 1% BSA, and 0.1% Na<sub>2</sub>S<sub>2</sub>O<sub>8</sub>). Cells were stained with the following antibodies: APC anti-mouse H-2Kb-SIINFEKL-specific antibody (BioLegend 141606), APC mouse IgG1,  $\kappa$  isotype control (BioLegend, 981806), APC rat anti-mouse CD8a (BD Biosciences, 553035), and APC mouse IgG2a  $\kappa$  isotype control (BD Biosciences, 550882). Cells were washed with FACS buffer, stained using the FITC-conjugated annexin V<sup>+</sup> apoptosis kit I (BD Pharmingen 556547), and analyzed using an Attune NxT flow cytometer. Staining protocols were performed according to the manufacturer's instructions, and data were analyzed using FlowJo software (version 10.9.0).

### B3Z T-cell hybridoma effect on E.G7-Ova viability

E.G7-Ova cells were pretreated for 24 or 48 hours with compounds (1  $\mu$ mol/L), after which they were washed with PBS and co-

cultured with B3Z cells at effector:target (E:T) ratios of 1:1, 2:1, and 3:1 for 16 hours. Co-cultures were then washed with PBS, resuspended in FACS buffer, and probed with antibodies to APC-conjugated rat anti-mouse CD8a, annexin V, and propidium iodide (PI) for 20 minutes. Cells were washed and analyzed using an Attune NxT flow cytometer. Apoptosis of E.G7-Ova cells was quantitated by gating for annexin V<sup>+</sup>, PI<sup>+</sup>, and CD8a<sup>-</sup> cells. Data were analyzed using FlowJo software (version 10.9.0).

### MS analysis of human and murine MHC-I antigens

In collaboration with MS Bioworks, MS was performed to isolate, sequence, identify, and quantitate the effect of compound A on MHC-I-bound antigenic peptides in E.G7-Ova and multiple myeloma cells (28). To determine the effect of compound A on the murine immunopeptidome, E.G7-Ova cells ( $5 \times 10^8$  cells/sample) were treated with compound A (1  $\mu$ mol/L) for 48 hours. To determine the effect of compound A on the myeloma immunopeptidome, RPMI-8226 cells ( $2 \times 10^8$ /sample) were treated with compound A (1  $\mu$ mol/L) for 48 hours. Cells were then washed with PBS and resuspended in lysis buffer (0.25% sodium deoxycholate, 200  $\mu$ mol/L iodoacetamide, 1% N-octyl- $\beta$ -D-thioglycoside, and 1  $\mu$ mol/L EDTA) containing protease inhibitor (1 mL lysis buffer/ $1 \times 10^8$  cells). Lysates were centrifuged at  $800 \times g$  for 5 minutes, the supernatant collected, additional lysis buffer added and mixed, and the mixture centrifuged at  $20,000 \times g$  for 60 minutes. The lysate was mixed with the H-2 MHC-I M1/42 antibody (2 mg in 100  $\mu$ L) for the murine immunopeptidome and the MHC-I W6/32 antibody (2 mg in 100  $\mu$ L) for the myeloma immunopeptidome. Lysates were mixed with the antibody resin, incubated overnight at 4°C with gentle rotation, centrifuged at  $800 \times g$  for 5 minutes, washed with lysis buffer, washed with buffer 2 (20 mmol/L Tris-HCl, and 400 mmol/L NaCl, pH 8.0), washed with buffer 3 (20 mmol/L Tris-HCl, and 150 mmol/L NaCl, pH 8.0), and washed with buffer 4 (20 mmol/L Tris-HCl, pH 8.0). Elution buffer (1 mL) was added to the resin and incubated for 5 minutes at 37°C. Eluted peptides were concentrated and desalted using solid-phase extraction with a Waters HPLC C18 column. Purified proteins were analyzed by LC/MS-MS using nanoscale chromatography with a Fusion Lumos mass spectrometer using electron-transfer/higher energy collision dissociation fragmentation. Peptides were loaded directly and eluted using 50/50 acetonitrile/water (0.1% trifluoroacetic acid). Eluted peptides were lyophilized, reconstituted in 0.1% trifluoroacetic acid, and analyzed by nano LC/MS-MS using a Waters NanoAcquity system interfaced to a Thermo Fisher Scientific Fusion Lumos mass spectrometer. Peptides were loaded on a trapping column and eluted over a 75- $\mu$ m analytical column at 350 nL/minute; both columns were packed with Luna C18 resin (Phenomenex). A 2-hour gradient was used. The mass spectrometer was operated using a custom data-dependent method, with MS performed in the Orbitrap at 60,000 FWHM resolution and sequential MS-MS performed using high-resolution collision-induced dissociation and electron-transfer higher-energy dissociation in the Orbitrap at 15,000 FWHM resolution. MS data were acquired from m/z 300 to 1600. A 3-second cycle time was employed for all steps. Raw files were searched using a local copy of PEAKS with the following parameters: Database: Swiss-Prot mouse oval-chick for murine immunopeptidome or Swiss-Prot human for the myeloma immunopeptidome; fixed modification: none; variable modifications: oxidation (M), acetyl (N-terminus), carbamidomethyl (C); mass values: monoisotopic; peptide mass tolerance: 10 ppm; fragment mass tolerance: 0.02 Da; max

missed cleavages: N/A; PSM FDR: 1%; and chimeric peptide: TRUE. Data were further processed using Skyline v22.2.0.255.

### NeoAg identification

To identify NeoAgs, posttranslational modification (PTM) profiling of peptides bound to human HLA-ABC molecules after immunoprecipitation was performed. PTM profiling was performed using a high-resolution approach that combined trypsin digestion with state-of-the-art LC/MS-MS, employing electron transfer dissociation, collision-induced dissociation, and higher energy collision-induced dissociated fragmentation regimes. PTMs detected included methylation, oxidation, phosphorylation, ubiquitination, acetylation, nitration, and mutation. Data were searched with the target PTM as a variable modification, common example PTMs, and product ion spectra. RPMI-8226 cells were treated with compound A, and lysates prepared and immunoprecipitated with a W6/32 antibody. MS was performed to sequence and identify eluted immunopeptides. The workflow provided deep sequence analysis of immunogenic peptides for the identification of NeoAgs.

### Western blotting

Cells were lysed using RIPA lysis and extraction buffer (Invitrogen, #89901) that contained protease and phosphatase inhibitor cocktail (Cell Signaling Technology, #5872). Protein concentration was measured using the Pierce Bradford protein assay kit (Invitrogen, #23200). Protein samples for SDS-PAGE were prepared by adding NuPAGE lithium dodecyl sulfate sample buffer (Invitrogen, #NP0007) and NuPAGE sample reducing agent (#NP0009). Samples were heated at 95°C for 3 minutes and protein (25 µg/sample) loaded into wells on NuPAGE 4% to 12%, Bis-Tris, 1.0 mm, mini protein gels (Invitrogen). NuPAGE MES SDS running buffer (Invitrogen, #NP0002) was used for resolving small- to medium-sized proteins and NuPAGE MOPS SDS running buffer (Invitrogen, #NP0001) used to resolve medium-large-sized proteins. After electrophoresis, proteins from NuPAGE Bis-Tris gels were transferred to polyvinylidene fluoride membranes (Bio-Rad, #1620177) using NuPAGE transfer buffer (Invitrogen, #NP00061). Membranes were blocked with Intercept blocking buffer (LI-COR) for 60 minutes followed by overnight incubation with primary antibodies (1:1,000 dilution) at 4°C. Membranes were washed thrice with PBS containing 0.1% Tween-20 prior to probing with the respective secondary antibodies (1:2,000 dilution). Membranes were imaged using a Li-COR system interfaced with the Odyssey-CLx and Imaging Studio 4.0 software.

### Native PAGE

Cells were lysed using native lysis buffer composed of 10% glycerol, 5 mmol/L MgCl<sub>2</sub>, 20 mmol/L Tris-HCL (pH 7.8), 20 mmol/L NaCl, 3 mmol/L ATP, and 1 mmol/L DTT. Lysates were resolved on a Native PAGE 3% to 6%, Bis-Tris, 1.0 mm, mini protein gels (Thermo-Fisher Scientific, #BN1001BOX) using a native running buffer composed of 1× Tris-borate EDTA supplemented with 3 mmol/L ATP, 5 mmol/L MgCl<sub>2</sub>, and 0.5 mmol/L DTT (29). Gels were transferred to polyvinylidene fluoride membranes, incubated with primary and secondary antibodies, and processed using a Li-COR imaging system interfaced with the Odyssey-CLx and Imaging Studio 4.0 software. Purified human 26S proteasomes (Life Sensors, #PS-0026-0050), 20S proteasomes from red blood cells (RnD systems, #E-360-050), and 20S

immunoproteasomes (South Bay Bio, #SBB-PP0004) were used as migration standards.

### Antibodies

Primary antibodies used were anti-PSMA1 Rb pAb (Thermo Fisher Scientific, PA1-963; 3 µg/mL); anti-PSME1 Rb mAb at 1:5,000 (Abcam, ab155091); anti-PSME2 pAb 1:5,000 (Thermo Fisher Scientific, 12937-2-AP); anti-PSME3 Rb pAb (Abcam, ab157157), 1:2,500 dilution; anti-PSME4 Rb pAb (Abcam, ab5620), 1:5,000; anti-POMP (D2X9S) Rb mAb (CST, 15141), 1:1,000; anti-PSMB5 Rb pAb (Abcam, ab3330), 1:1,000; anti-PSMB6 (E1K9O) Rabbit mAb (CST, 13267), 1:1,000 dilution; anti-PSMB7 (E1L5H) rabbit mAb (CST, 13207), 1:1,000 dilution; anti-20S LMP7/PSMB8 Rb mAb (Abcam, ab180606), 1:10,000; anti-20S LMP2/PSMB9 Rb pAb (Abcam, ab42987), 1:1,000; anti-PSMB10 mouse mAb (Abcam, ab77735), 1:100; anti-FLAG mouse mAb (MilliporeSigma, F1804-50UG; 1 µg/mL); anti-β-actin (8H10D10) mouse mAb (CST, 3700), 1:1,000; and anti-GAPDH (D4C6R) mouse mAb (CST, 97166) at 1:1,000.

Secondary antibodies were IRDye 800CW donkey anti-rabbit IgG (Li-Cor 926-32213), IRDye 800CW goat anti-mouse IgG (Li-Cor 926-32210), IRDye 680LT donkey anti-rabbit IgG (Li-Cor 926-68023), and IRDye 680LT goat anti-mouse IgG secondary antibody (Li-Cor 926-68020).

### Effect of compound A on HLA allelic subtypes on multiple myeloma cells

MMCLs were treated for 48 hours with compound A (1 µmol/L), after which cells were PBS washed twice, resuspended in FACS buffer, and probed with antibodies to the following: HLA-ABC (W6/32), recombinant Alexa Fluor 647-conjugated anti-HLA-A (Abcam, ab199837), HLA-B (Invitrogen, PA5-35345), and Alexa Fluor 647-conjugated anti-human HLA-C (BioLegend, 373308). RPMI-8226 cells were also probed using an HLA-A antigen-specific A30, A31 mAb (MyBioSource, MBS602344) and the MHC-I antigen B15 polyclonal antibody (Bioss, BS-4120R). U266 cells were also probed using APC-conjugated anti-human HLA-A2 antibody (BioLegend, 343308) and PE-conjugated HLA-B7 mAb (BB7.1; Invitrogen, 12-5917-42).

### Effect of compound A on allogeneic T-cell-mediated myeloma lysis

Cells were treated for 48 hours with compound A (1 µmol/L), washed with PBS, and co-cultured with CD8<sup>+</sup> T cells (E:T of 1:1, 2:1, and 3:1) for 16 hours. Co-cultures were probed using antibodies to Alexa Fluor 647-conjugated mouse anti-human CD138 (BD Pharmingen, 562097), FITC-conjugated annexin V (BD Pharmingen, 556419), and PI (BD Pharmingen, 556463) to quantitate apoptotic tumor cells. Cells were washed and analyzed using an Attune NxT flow cytometer.

### Autologous T-cell-mediated patient CD138<sup>+</sup> cell apoptosis

Bone marrow from patients with multiple myeloma was obtained after informed consent as described in the Institutional Review Board-approved protocol. CD138<sup>+</sup> cells were isolated from patient bone marrow using the EasySep Human CD138 positive selection kit II (StemCell Technologies, #17877) according to the manufacturer's guidelines. Autologous CD8<sup>+</sup> T cells were isolated from peripheral blood mononuclear cells of patients with multiple myeloma using the CD8<sup>+</sup> T-cell isolation kit (Miltenyi Biotec, #130-096-

495). CD138<sup>+</sup> cells were treated with compound A (1  $\mu$ mol/L) for 24 hours, washed, and co-cultured with autologous CD8<sup>+</sup> T cells at an E:T of 2:1 for 18 hours. Autologous CD8<sup>+</sup> T-cell-mediated cytotoxicity was measured by gating for CD138<sup>+</sup>, annexin V<sup>+</sup>, and PI<sup>+</sup> cells.

#### Effect of compound A on PDL1/PDL2 expression on MMCLs

RPMI-8226, ARH-77, and U266 were treated with compound A (1  $\mu$ mol/L), TGF $\beta$ 1 (10 ng/mL), or bortezomib (10 nmol/L) for 24 hours. Cells were washed in PBS, resuspended in FACS buffer, and stained using PDL1 antibody FITC anti-human CD274 B7-H1, PDL1 antibody (BioLegend #393606), and PDL2 antibody APC anti-human CD273 B7-DC (BioLegend #345508). PDL1 and PDL2 levels were quantitated using an Attune flow cytometry integrated with FlowJo software (version 10.9.0).

#### Effect of compound A combined with ICIs on T-cell cytotoxic activity

RPMI-8226, ARH-77, and U266 cells were pretreated with compound A (1  $\mu$ mol/L), after which they were co-cultured with healthy human CD8<sup>+</sup> T cells (HumanCells Biosciences) alone or with pembrolizumab (5  $\mu$ g/mL, SelleckChem), nivolumab (10  $\mu$ g/mL, SelleckChem), durvalumab (20  $\mu$ g/mL, SelleckChem), atezolizumab (20  $\mu$ g/mL, SelleckChem), bortezomib (10 nmol/L), or TGF $\beta$ 1 (10 ng/mL, PeproTech) for 18 hours. The effect of CD8<sup>+</sup> T cells alone and with ICIs, proteasome inhibitors, or TGF $\beta$ 1 was determined by gating for CD138<sup>+</sup>/annexin V<sup>+</sup>/PI<sup>+</sup> cells.

#### E.G7-Ova GFP-luciferase-expressing cells

Lentiviral vector pLV[exp]-EGFP:T2A:Puro-EF1A>luciferase containing a GFP and firefly luciferase (*Luc*) fusion gene was from VectorBuilder (VB900084-0155eck). The gene cassette was cloned into a lentiviral expression vector containing a puromycin resistance gene under an EF1A promoter. Lentiviral particles were produced by co-transfection vector with packaging plasmids pRSV-Rev (Addgene, #12253), pMDLg/pRRE (Addgene, #12251), and pMD2.G-VSVG (Addgene, #12259) in HEK293T cells using lipofectamine. The supernatant containing lentiviral particles was collected 53 hours post-transfection, filtered through a 0.45- $\mu$ m PES filter. E.G7-Ova cells were transduced with lentiviral particles carrying the GFP-Luc expression construct. Cells were seeded at  $5 \times 10^5$  cells/mL in a T175 flask and incubated with lentiviral supernatant with polybrene (8  $\mu$ g/mL). After 16 hours, media was replaced and puromycin (10  $\mu$ g/mL, Sigma-Aldrich) added to the transduced E.G7-Ova cells to select and establish a stable cell line expressing the GFP-Luc fusion protein. Cells were maintained in puromycin-containing medium for  $\geq 1$  week to ensure the establishment of a stable, drug-resistant population. Cells were imaged using an inverted fluorescence microscope for GFP expression, and luciferase activity was assessed using a luciferase assay kit (Promega) and luminometer.

#### Effect of compound A pretreatment on tumor implants *in vivo*

Mouse studies were approved by the Institutional Animal Care and Use Committee. OT-1 mice were obtained from Jackson Laboratory and housed in a controlled environment with a 12-hour light–dark cycle. OT-1 mice contain transgenic inserts for mouse *Tcra-V2* and *Tcrb-V5* genes. The transgenic TCR recognizes Ova residues 257 to 264 in the context of H2K<sup>b</sup> (CD8 co-receptor interaction with MHC-I). This results in MHC-I-restricted, Ova-specific, CD8<sup>+</sup> T cells in OT-1 mice. Mice had *ad*

*libitum* access to alfalfa-free rodent chow and water. Animals were acclimated for 2 days before experimental procedures. E.G7-Ova-GFP-Luc expressing cells were harvested during the logarithmic growth phase and viability confirmed with trypan blue. OT-1 mice were segregated into two groups (four/group) and anesthetized with isoflurane, and  $5 \times 10^6$  E.G7-Ova-GFP-Luc cells in 100  $\mu$ L PBS were intraperitoneally injected. Prior to injection, E.G7-Ova-GFP-Luc cells were treated with vehicle (0.05% DMSO) or compound A (1 mmol/L) for 24 hours. Tumor volume was measured using digital calipers and reported as the product of the two largest perpendicular diameters (mm<sup>2</sup>). Mice were monitored daily for general health, activity level, and signs of distress throughout the experiment. Any abnormalities, including weight loss, change in behavior, or signs of illness, were recorded and veterinary care was sought. For all needed experimental procedures, mice were anesthetized with isoflurane using a precision vaporizer.

#### Bioluminescence imaging

For *in vivo* imaging, mice were injected with D-luciferin (Revvity) intraperitoneally. After a 10-minute distribution period, images were acquired using the Spectrum IVIS System. Exposure time and f-stop were adjusted as necessary. Serial imaging was performed at specified time points post-injection.

#### Region of interest measurement

Bioluminescence imaging (BLI) data were analyzed using Living Image Software (Revvity). Regions of interest (ROI) were manually drawn around tumor areas on acquired images, and BLI within defined ROIs was quantified. Data were expressed as photon flux (photons/second) for each ROI. Data normalization was performed based on controls or background signals, as indicated.

#### Total body weight

Total body weight (TBW) was measured on indicated days using digital calipers.

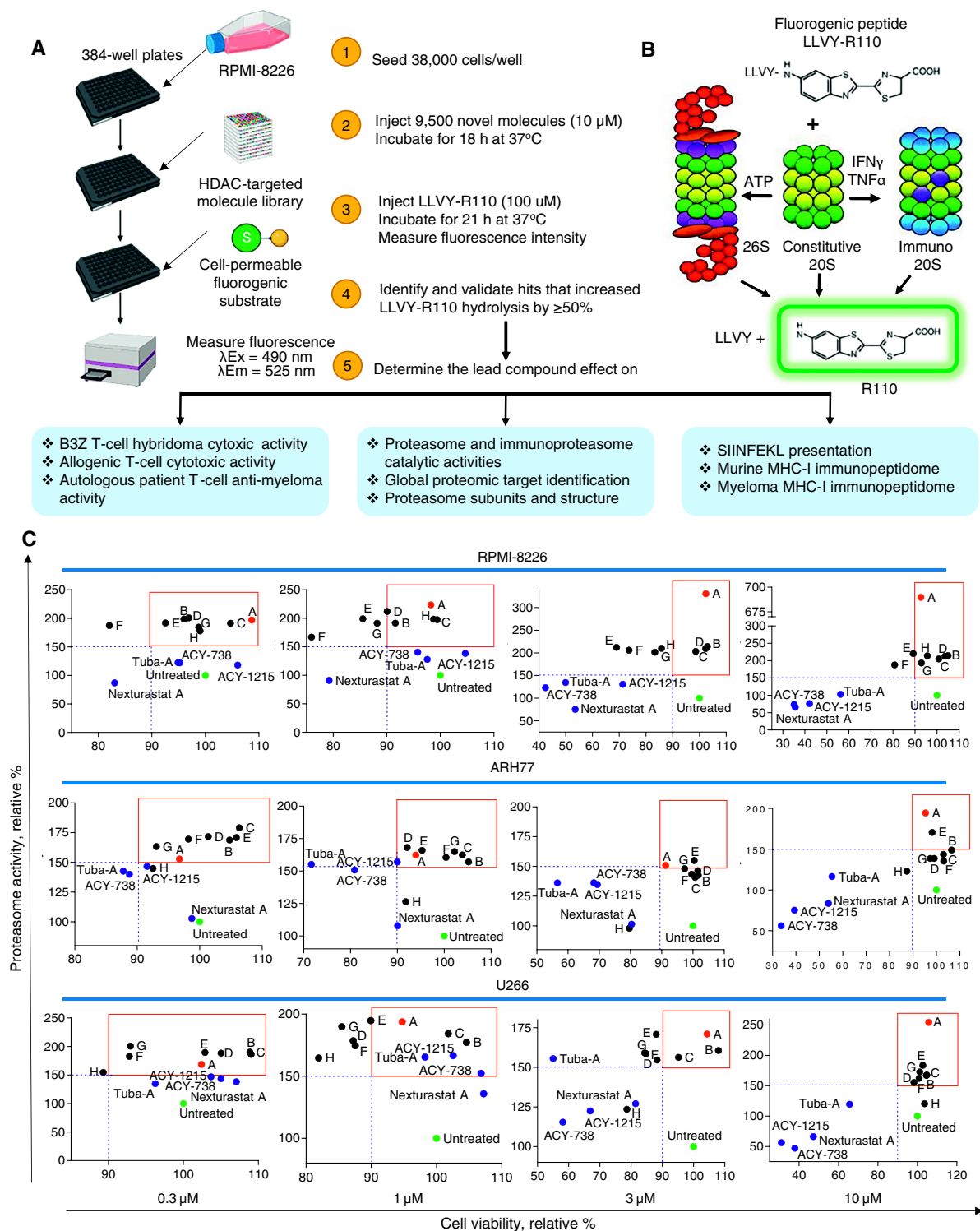
#### Quantification and statistical analysis

Assays were performed in triplicate unless indicated otherwise. Population frequencies exported from FlowJo were analyzed for statistical significance using GraphPad Prism Software 8.4.1 (GraphPad) or Microsoft Excel. Summary plots were prepared using GraphPad Prism 10.1.0 (316) or Excel. Significant differences were accounted for using the two-sided student *t* test (Excel). For individual tests, a *P* value  $\leq 0.05$  was considered significant. *P* values were calculated and reported as follows: ns: not significant; \*, *P*  $\leq 0.05$ ; \*\*, *P*  $\leq 0.01$ ; \*\*\*, *P*  $\leq 0.001$ . Error bars in each figure represent the relative SEM. A one-way ANOVA (equal SDs) assessed the statistical significance for Fig. 7C. *P* values from log-rank (Mantel–Cox) test and HR of the respective groups, including 95% confidence intervals (CI) and Kaplan–Meier survival probability, were calculated using GraphPad Prism Software 8.4.1. Data and materials are available upon request from J.J. Driscoll.

## Results

### High-throughput screens to identify novel compounds that increase proteasomal activity

We screened a library of 9,500 molecules to identify those that increased proteasomal ChT-like activity in RPMI-8226 cells (Fig. 1A). The effect on activity was determined by measuring the fluorescence intensity produced upon cleavage of the cell-permeable

**Figure 1.**

Identification of novel molecules that increased proteasomal ChT-like activity. **A**, Schematic representation of the cell-based HTS. RPMI-8226 cells were treated with a library of 9,600 novel molecules and the effect on proteasomal ChT-like activity measured. Top hits were identified that increased proteasome ChT-like activity by  $\geq$ 50%, and the selected primary hits were further evaluated for their effects on cell viability, antigen presentation, and T-cell-mediated cytotoxicity in murine and human cell-based assays. **B**, Schematic of the HTS using the cell-permeable fluorogenic substrate LLVY-R110 that is specifically cleaved by proteasomes and immunoproteasomes. **C**, Effect of the hits on cell viability and proteasome activity in RPMI-8226, ARH-77, and U266 cells. Red boxes indicate compounds that increased proteasome activity  $\geq$ 50% and maintained cell viability  $\geq$ 90%. HTS, high-throughput screens; tuba-A, tubastatin A.

fluorogenic substrate LLVY-R110, which is cleaved by both constitutive proteasomes and immunoproteasomes (Fig. 1B). We identified eight molecules (compounds A–H) that increased LLVY-R110 cleavage by  $\geq 50\%$  (Supplementary Fig. S1–S3). The eight hits, which represented 0.09% of the total number of molecules screened, were analyzed for an effect on cell viability. RPMI-8226, ARH-77, and U266 cells were incubated with each compound at the indicated time and concentration. Treatment with most compounds at 1  $\mu\text{mol/L}$  for 48 hours maximally increased LLVY-R110 cleavage and maintained cell viability  $>90\%$ . Previously, we had demonstrated that treatment of multiple myeloma cells with HDAC6 inhibitors promoted proteasomal ChT-like activity (30). We compared the effects of compound A with the HDAC6-specific inhibitors tubastatin A, ACY-738, ACY-1215, and nexturastat A. In contrast to known HDAC6 inhibitors, compound A did not inhibit HDAC6 enzymatic activity (Supplementary Table S1). Also, compounds A, B, and C increased ChT-like activity to a greater extent than the HDAC6 inhibitors (Fig. 1C).

### Compound A specifically promotes immunoproteasome activity

The 26S proteasome is composed of two subcomplexes: a 20S catalytic core particle capped at either or both ends by 19S regulatory particles that confer ATP and Ub-dependence (31). The constitutive 20S proteasome catalytic subunits are  $\beta 1$ ,  $\beta 2$ , and  $\beta 5$  (encoded by *PSMB6*, *PSMB7*, and *PSMB5*), which are expressed in all cells. In response to IFN $\alpha/\beta$  or  $\gamma$  and TNF, there is an increase in the immunoproteasome catalytic subunits  $\beta 1i/LMP2$ ,  $\beta 2i/MECL-1$ , and  $\beta 5i/LMP7$  (encoded by *PSMB9*, *PSMB10*, and *PSMB8*). Owing to the complex subunit structure of proteasomes and variants, we investigated the effect of compound A on substrate specificity. We measured the effect on individual proteasomal catalytic activities by monitoring the hydrolysis of fluorogenic peptides that are specifically cleaved by individual proteasome or immunoproteasome active sites. Suc-LLVY-AMC and LLVY-R110 are cleaved by active sites within both  $\beta 5$  and  $\beta 5i$ , whereas Ac-ANW-AMC fluoresces specifically after cleavage by  $\beta 5i$  and is not cleaved by  $\beta 5$ . Treatment of RPMI-8226 cells with compound A increased the hydrolysis of Suc-LLVY-AMC and LLVY-R110 by  $>1.5$ -fold compared with vehicle-treated controls (Fig. 2A). Treatment of HeLa cells with compound A did not significantly increase hydrolysis of the same substrates relative to controls (Fig. 2B). Under basal conditions, for example, in the absence of IFN $\gamma$  or TNF, HeLa cells are devoid of immunoproteasomes, and, hence, no change in ChT-like activity was observed after treatment of cells with compound A. RPMI-8226 cells were then treated with compound A or vehicle, lysates were generated, and the hydrolysis of a series of substrates specifically cleaved by proteasome and immunoproteasome active sites were measured (Fig. 2C). Compound A enhanced the hydrolysis of the  $\beta 5i$ -specific substrate Ac-ANW-MCA by 2.5-fold. Compound A did not alter the hydrolysis of substrates cleaved by the  $\beta 1$ ,  $\beta 2$ ,  $\beta 1i$ , and  $\beta 2i$  subunit active sites.

Selective immunoproteasome inhibition has been shown to have unique effects on a number of diseases, including those involving aberrant immune function (32, 33). ONX-0914 is an inhibitor of the LMP7 and LMP2 subunits of immunoproteasomes and has activity in multiple models of autoimmune diseases in mice. ONX-0912 (oprozomib, PR-047) is an orally bioavailable inhibitor for ChT-L activity of 20S immunoproteasome  $\beta 5i$  subunit. KZR-616, a derivative of ONX-0914, has been evaluated in clinical trials for the treatment of lupus. Multiple myeloma cells were treated with each

of the three immunoproteasome-specific inhibitors with and without co-treatment with compound A and the effect on cell viability determined (Fig. 2D). At concentrations  $\leq 10$  nmol/L, the immunoproteasome inhibitors did not reduce cell viability. However, treatment of multiple myeloma cells with each immunoproteasome inhibitor reduced the hydrolysis of Ac-ANW-MCA in a dose-dependent manner (Fig. 2E and F). Importantly, the immunoproteasome-specific inhibitors blocked the effect of compound A on immunoproteasome-specific catalytic activity.

### Compound A binds PSMA1 to increase immunoproteasome activity

RPMI-8226 cells were treated with compound A at 6 and 24 hours; lysates were processed with PISA. Four proteins detected in both time points (6 and 24 hours) demonstrated differential stabilization ( $P$  value  $\leq 0.05$ ) compared with vehicle samples and had unchanged abundance levels in the paired global proteomics experiments (Fig. 3A). Proteins interacting with the tested molecules (targets and off-targets), the activated factors, or proteins modified during the treatment show reproducible changes in their soluble amount compared with vehicle-treated controls (34, 35). Proteasome subunit  $\alpha$  type-1, encoded by *PSMA1*, is essential to the assembly of 20S proteasomes. *PSMA1*, a known binding partner of the PA28 $\alpha/\beta$  proteasome activator, is expressed by *PSME1* and *PSME2*. *PSMA1*, *PSME1*, and *PSME2* were silenced using sgRNA in RPMI-8226 and ARH-77 cells (Fig. 3B). Silencing of each gene abolished the effect of compound A on Ac-ANW-MCA hydrolysis in cell lysates.

### Compound A increases presentation of murine H2Kb MHC-I-SIINFEKL

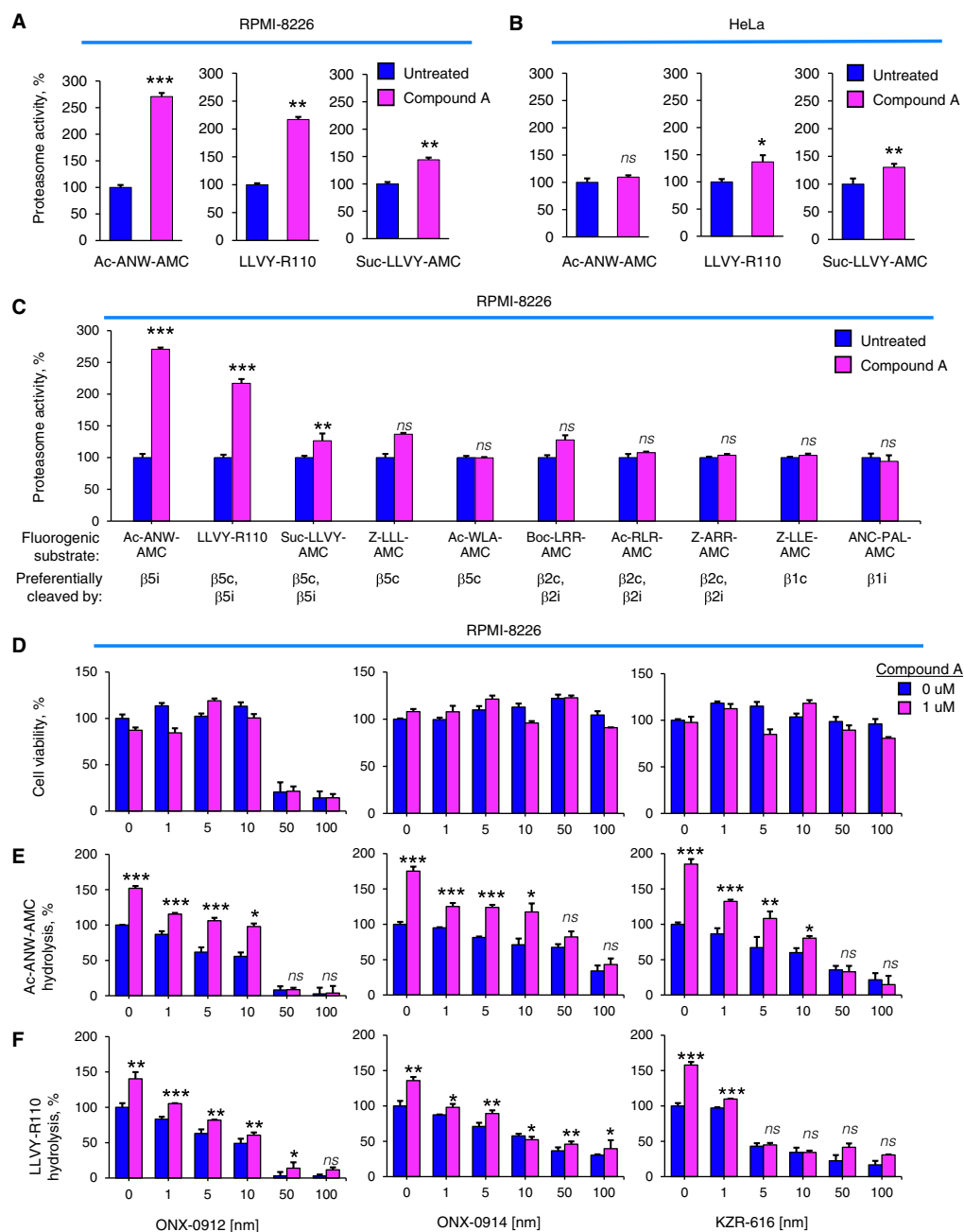
We determined the effect of each hit on proteasome activity, cell viability, MHC-I antigen presentation, and CTL-mediated tumor cell lysis using E.G7-Ova cells. E.G7-Ova cells have been genetically modified to constitutively synthesize Ova, which upon proteasomal degradation generates the antigenic peptide SIINFEKL OVA (257–264), which is presented by H2Kb (36). Pretreatment of E.G7-Ova cells with each compound maintained cell viability, whereas compound A was the most effective and increased MHC-I-SIINFEKL presentation by six-fold (Supplementary Fig. S4A and S4B).

### Compound A promotes B3Z-mediated E.G7-Ova lysis

E.G7-Ova cells were treated with the indicated compounds, after which they were washed and co-cultured with B3Z cells. The B3Z T-cell hybridoma expresses a TCR that specifically recognizes SIINFEKL complexed with H-2Kb (37). Compound A was the most potent compound to induce B3Z-mediated lysis of E.G7-Ova cells at each point assayed (Fig. 4A; Supplementary Fig. S4C).

### Treatment of EG.7-Ova cells with compound A expands the murine immunopeptidome

We next determined the effect of compound A on the global MHC-I immunopeptidome of E.G7-Ova cells. Peptides eluted from MHC-I molecules were identified and screened for their abundance, diversity, copy number, length, amino acid sequence, HLA alleles, and gene source. A total of 1,090 peptides were eluted from cells treated with compound A compared with 883 peptides eluted from the untreated cells (Fig. 4B). Peptide peak intensity was  $\sim 2$ -fold higher in compound A-treated cells than in controls treated with vehicle (Fig. 4C). The peak area of  $\sim 450$  eluted peptides was  $\geq 2$ -fold greater after treatment with compound A. The relative level of

**Figure 2.**

Effect of compound A on proteasomal catalytic activities. **A**, Effect of compound A on proteasomal peptide-hydrolyzing activity in RPMI-8226 cells. Cells were treated with the fluorogenic peptide substrates Suc-LLVY-MCA, LLVY-R110, and Ac-ANW-MCA for 1 to 3 hours. Fluorescent intensity was monitored as a direct measurement of substrate hydrolysis. **B**, Effect of compound A on proteasomal peptide-hydrolyzing activity in HeLa cells. **C**, Effect of compound A on a series of fluorogenic substrates specifically cleaved by proteasome and immunoproteasome catalytic sites. LLVY-R110 and Suc-LLVY-MCA are cleaved by both the  $\beta 5c$  subunit and  $\beta 5i$  subunit, whereas ANC-ANW-AMC is cleaved specifically only by the  $\beta 5i$  subunit. Z-LLL-AMC is cleaved by  $\beta 5c$ , Ac-WLA-AMC is cleaved by  $\beta 5c$ , Boc-LRR-AMC is cleaved by the  $\beta 2c$  and  $\beta 2i$  subunits, Ac-RLR-AMC is cleaved by the  $\beta 2c$  and  $\beta 2i$  subunits, Z-ARR-AMC is cleaved by the  $\beta 1c$  subunit, and ANC-PAL-AMC is cleaved by the  $\beta 1i$  subunit. Lysates from RPMI-8226 cells were incubated with the indicated proteasome substrates at concentrations of 15  $\mu\text{mol/L}$  for up to 3 hours, and fluorescent intensity monitored was a direct measure of the activity of proteasomal subunit-specific catalytic activity. **D**, Effect of immunoproteasome-specific inhibitors on multiple myeloma viability as determined by the 2,3-bis[2-methoxy-4-nitro-5-sulfophenyl]-2H-tetrazolium-5 carboxanilide inner salt assay. **E** and **F**, Effect of treatment with immunoproteasome-specific inhibitors on the ability of compound A to modulate proteasomal catalytic activity in multiple myeloma cells. RPMI-8226 cells were treated with the immunoproteasome inhibitors ONX-0912, ONX-0914, and KZR-616 at the indicated concentrations with and without compound A. Proteasomal ChT-like activity was then measured by recording LLVY-R110 hydrolysis as mentioned earlier. Immunoproteasome-specific activity was measured by recording Ac-ANW-AMC hydrolysis. Bioassays were performed in triplicate.

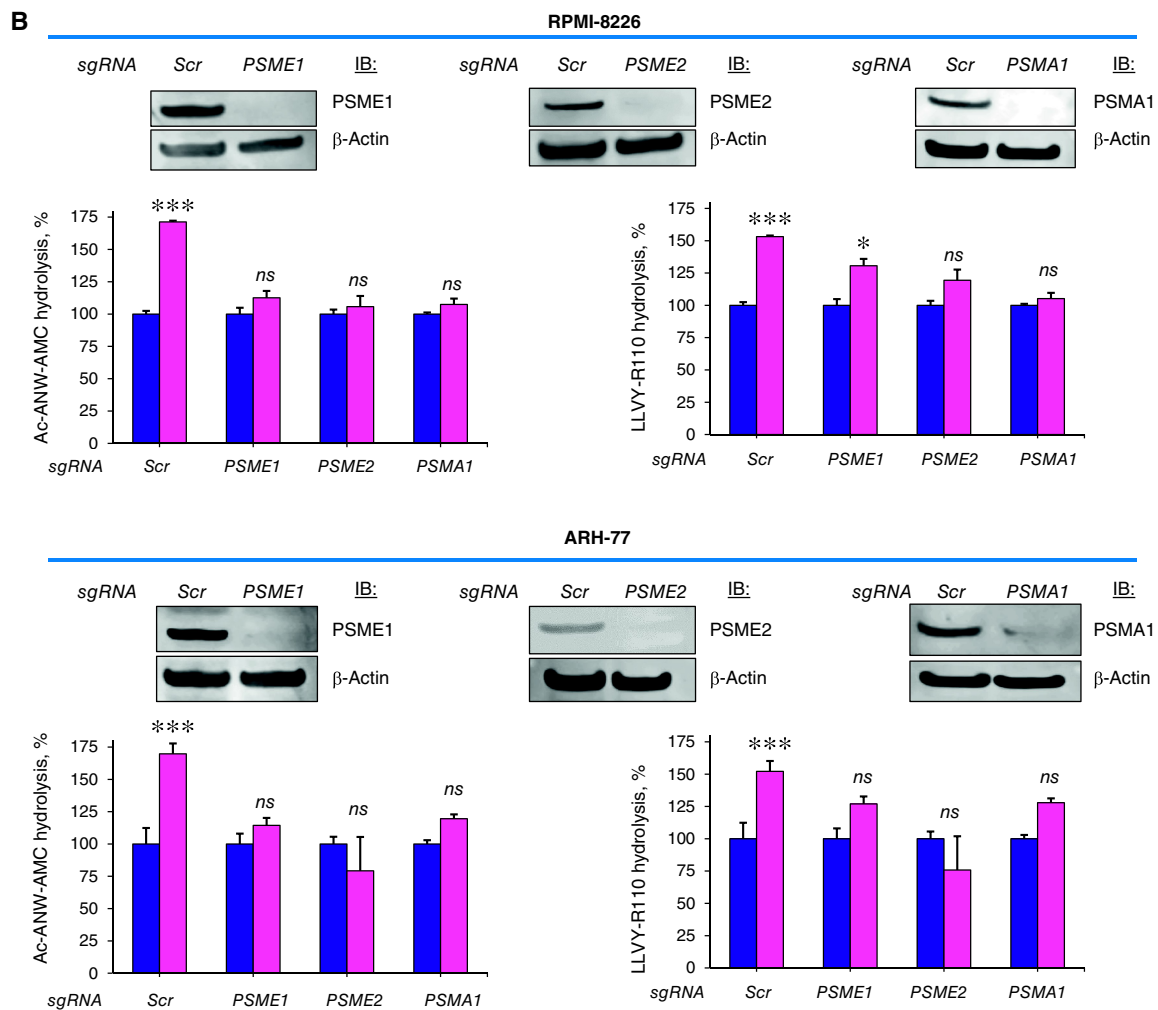
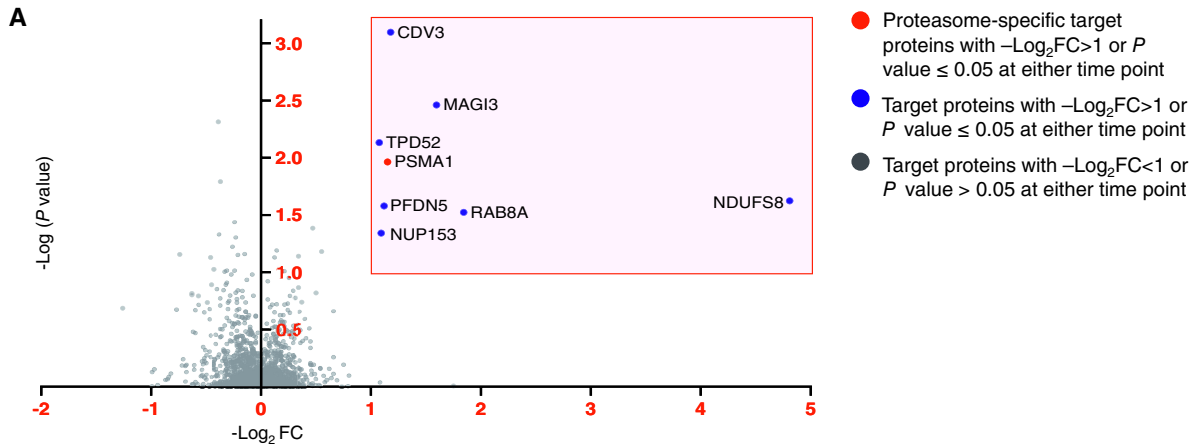


**Figure 3.**

Global PISA assay to identify compound A target proteins. Results of 1D PISA identified four proteins that demonstrated statistically significant  $P$  values after treatment at both 6 and 24 hours compared with vehicle samples. Red box indicates the most significantly stabilized target proteins following treatment of RPMI-8226 cells with compound A after both 6 and 24 hours. The proteasome-specific protein PSMA1 is indicated by a red dot. Gray dots indicate proteins with  $-\text{log}_2\text{FC} < 1$  or  $P$  value  $> 0.05$  at either time point. **B**, Effect of *PSME1*, *PSME2*, and *PSMA1* on the effect of compound A on proteasome activity. Effect of compound A on immunoproteasome activity was measured using Ac-ANW-AMC in cells with KO of *PSME1*, *PSME2*, and *PSMA1*. Immunoblots show CRISPR/CAS9-mediated *PSME1*, *PSME2*, and *PSMA1* KO in RPMI-8226 and ARH-77 cells followed by the effect on proteasomal catalytic activities. IB, immunoblot; KO, knockout.

SIINFEKL peptide eluted from MHC-class I (M1/42) molecules was ~2-fold higher after compound A treatment compared with vehicle treated controls, whereas SIINFEKL peptide copy number/cell was increased three-fold by compound A (Fig. 4D and E). The distribution of the length of peptides eluted from MHC-I (M1/42) molecules was not altered by compound A, and most eluted peptides were 8 to 9 amino acids in length (Fig. 4F). Importantly, the peak area value of certain individual peptides was increased as much as 200-fold following treatment with compound A (Fig. 4G). The amino acid sequence and gene source of the 20 most upregulated MHC-I-bound peptides increased after compound A treatment, which is shown in Fig. 4H.

### Compound A expands and diversifies the myeloma immunopeptidome

As compound A potentially amplified the murine MHC-I immunopeptidome, we investigated the effects of compound A on the global immunopeptidome of multiple myeloma cells. RPMI-8226 cells were treated with compound A (1  $\mu$ mol/L, 48 hours), lysates generated, MHC-I complexes immunoprecipitated using a pan-MHC antibody, and antigenic peptides eluted. A total of 5,368 peptides were eluted from the cells treated with compound A as compared with 4,063 peptides eluted from control-treated cells (Fig. 5A). Peptide peak intensity was ~2-fold greater in compound A-treated cells than in controls (Fig. 5B). A histogram distribution indicated that the length of peptides eluted from the MHC-I (W6/32) molecule was not altered by compound A and that the eluted peptides were primarily nine amino acids in length (Fig. 5C). The peak area value of >2,200 peptides was two-fold greater after treatment with compound A, whereas the peak area value of certain individual peptides was ~200-fold greater (Fig. 5D). A waterfall histogram representing the fold change in cells treated with compound A or bortezomib relative to the untreated cells is presented in Fig. 5D. Bortezomib treatment reduced the peak area of >1,500 peptides  $\geq$ 2-fold compared with that of untreated cells (Fig. 5E). After treatment with compound A, the relative number of the most upregulated peptides that terminated in either Tyr or Phe was consistent with an increase in immunoproteasome-specific activity (Fig. 5F). The amino acid sequence and gene source of the 20 peptides most upregulated or downregulated after treatment with compound A and bortezomib, respectively, are shown in Fig. 5G. A number of peptides downregulated by bortezomib were upregulated by compound A. The amino acid sequence and gene source of the 20 most upregulated peptides after compound A treatment are shown in Fig. 5H.

TAAgs are elevated on tumor cells and may be tumor-specific (38), whereas NeoAgs (tumor-specific antigens) are a repertoire of peptides that arise as the result of DNA mutations, PTM, and include antigens produced by tumor viruses integrated into the tumor cell genome (39). Unlike TAAgs, NeoAgs are truly foreign antigenic peptides and are entirely absent from normal human organs or tissues. An increase in TAAgs and NeoAgs was observed in cells treated with compound A (green arrow), whereas a decrease (red arrow) or absence (-) of peptide abundance was observed with bortezomib-treated cells. Over 25 TAAgs were significantly upregulated by compound A treatment. TAAgs upregulated by compound A treatment of multiple myeloma cells or downregulated by bortezomib treatment are shown (Supplementary Table S2). NeoAgs generated through mutation or PTM and upregulated following compound A treatment or

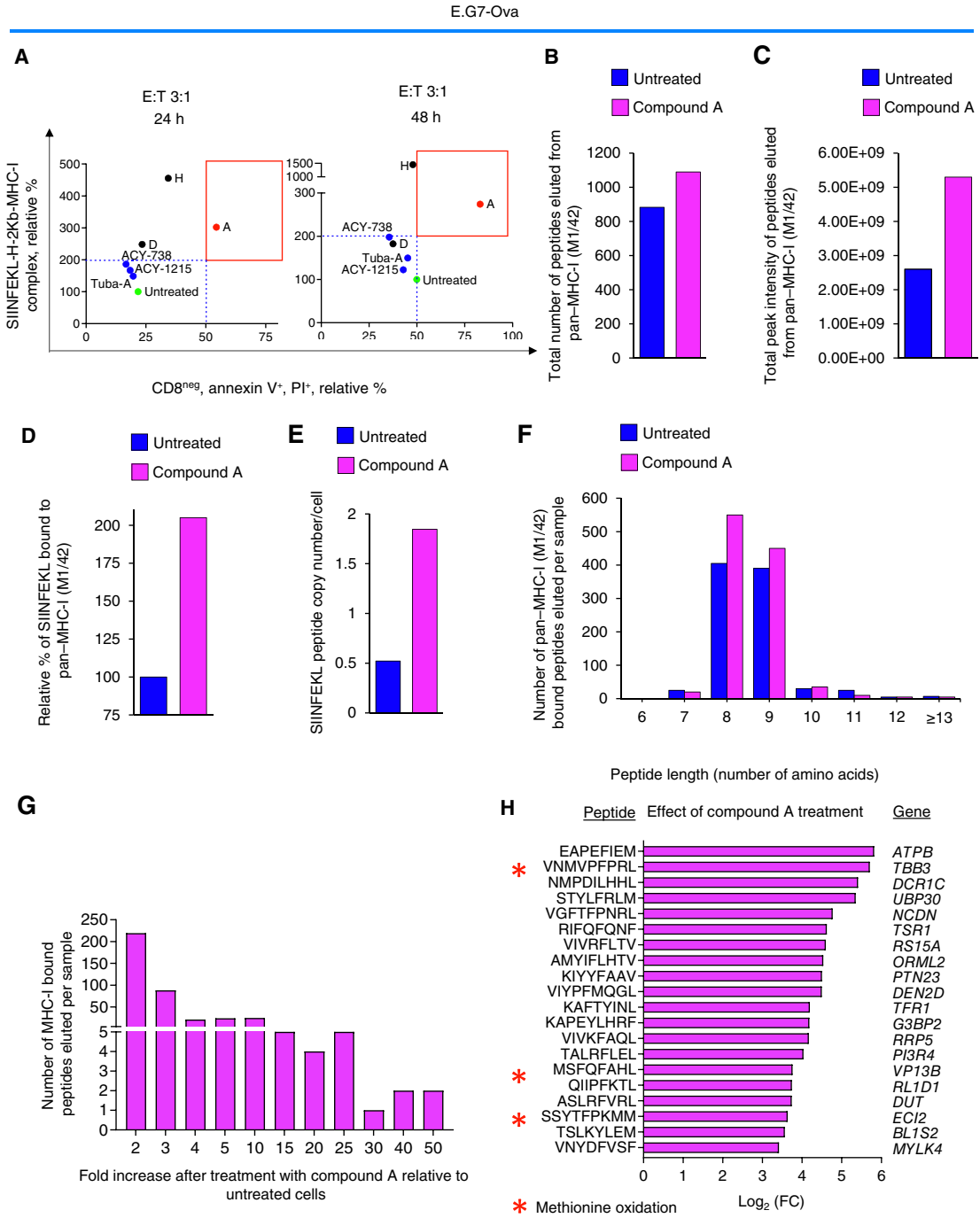
downregulated following bortezomib treatment are also shown (Supplementary Table S3). Importantly, many TAAgs upregulated by compound A treatment were downregulated by bortezomib treatment. Many TAAgs upregulated by compound A have previously been identified as cancer drivers, for example, RAF/BRAF, MUC1, CD28, and CDK6 (40–43).

### Compound A increases immunoproteasome catalytic and regulator subunits

As treatment with compound A specifically increased immunoproteasome catalytic activity, we determined the effect of compound A on individual proteasome catalytic and regulatory subunits. Treatment of multiple myeloma cells with compound A upregulated the  $\beta$ 5i subunit by 1.6-fold but did not change the level of other proteasome or immunoproteasome catalytic subunits in multiple myeloma lysates (Fig. 6A). Compound A treatment also increased the levels of PA28 $\alpha$ /PSME1 by three-fold and PA28 $\beta$ /PSME2 levels five-fold (Fig. 7B). Multiple myeloma cells were then transfected with vectors that expressed FLAG-tagged forms of either  $\beta$ 5/PSMB5 or  $\beta$ 5i/PSMB8. Compound A preferentially enhanced the binding of PA28 $\alpha$ / $\beta$  to FLAG-tagged  $\beta$ 5i compared with that bound to FLAG-tagged  $\beta$ 5 (Fig. 6C). Multiple myeloma cells were then treated with compound A and lysates prepared. The cell lysates were electrophoresed under non-denaturing conditions and probed with antibodies specific to either  $\beta$ 5/PSMB5 or  $\beta$ 5i/PSMB8 (Fig. 6D). Immunoblots indicated that compound A selectively increased the relative incorporation of  $\beta$ 5i/PSMB8, but not  $\beta$ 5/PSMB5, into endogenous 20S and 26S proteasomes. Compound A treatment also preferentially increased the level of FLAG-tagged  $\beta$ 5i/PSMB8-containing complexes (Fig. 6C, F, and G).

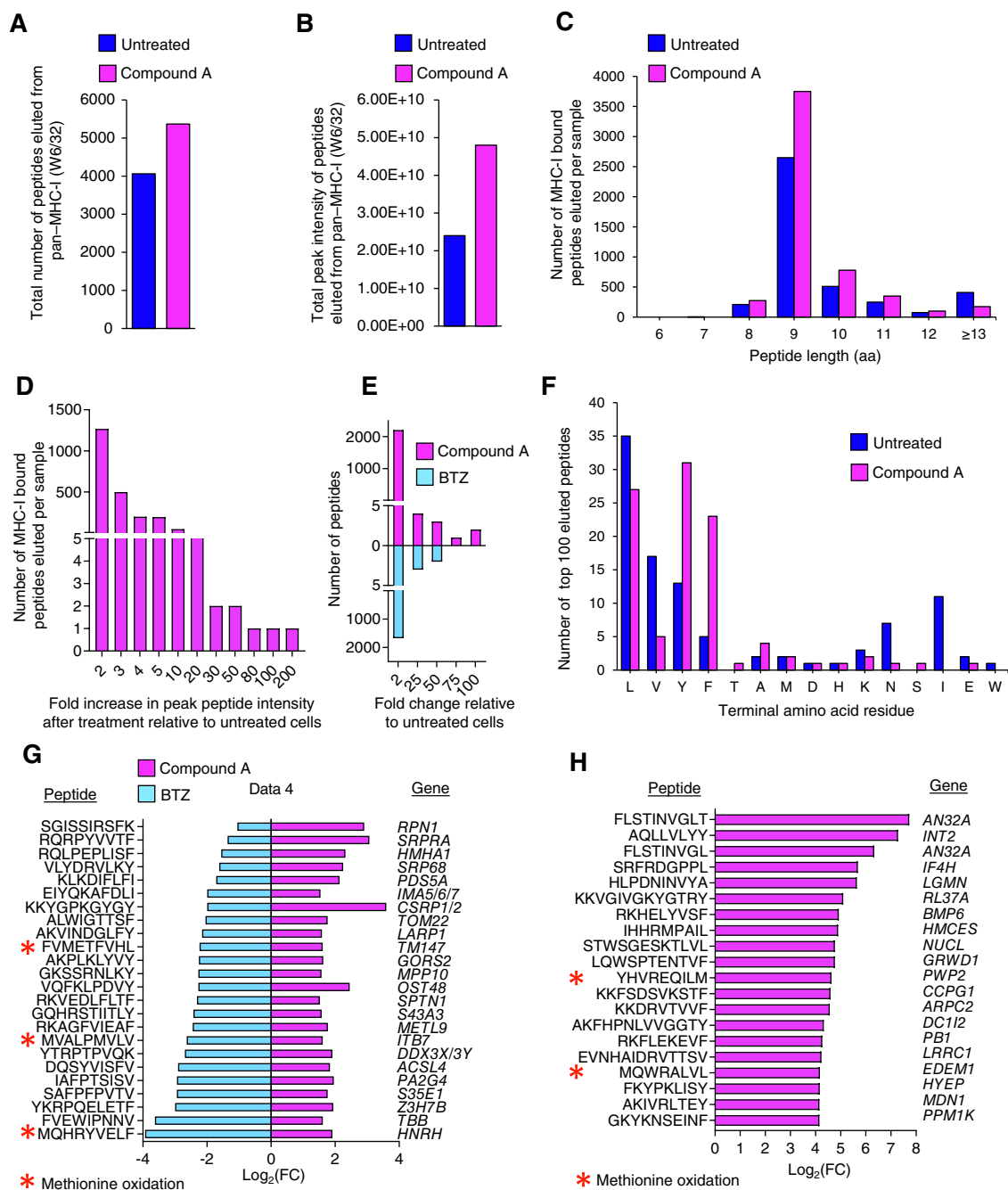
### Compound A promotes anti-myeloma activity of allogeneic and autologous CTLs

MMCLs were treated with compound A and the effect on pan- and individual HLA allele levels probed by antibody-specific staining and flow cytometry. Compound A treatment significantly increased the presentation of pan-HLA-ABC (W6/32) by ~1.6-fold ( $P = 0.0003$ ) in RPMI-8226, ARH-77, and U266 cells (Fig. 7A; Supplementary Fig. S5A). Treatment of RPMI-8226 cells with compound A increased HLA-B presentation by ~2-fold ( $P = 0.01$ ), the HLA-A  $\times$  30 subtype by 1.5-fold ( $P = 0.0001$ ), and the HLA-B15 subtype by 1.8-fold ( $P = 0.01$ ). Treatment of ARH-77 cells with compound A increased the presentation of HLA-B by 1.6-fold ( $P = 0.005$ ), with no significant change in HLA-A or HLA-C. Treatment of U266 cells with compound A significantly increased the presentation of HLA-B by 2-fold ( $P = 0.04$ ) and HLA-B15 subtype by 1.8-fold ( $P = 0.01$ ), with no significant change in HLA-C or the HLA-A  $\times$  02 subtype (Supplementary Fig S5A). Overall, compound A treatment enhanced the presentation of HLA-B and respective subtype alleles. MMCLs were pretreated with compound A and probed for the effect on apoptosis mediated by healthy, human allogeneic CD8<sup>+</sup> cytotoxic T cells. Multiple myeloma cells were incubated with T cells at E:T ratios of 1:1, 2:1, and 3:1 and T-cell-mediated tumor lysis analyzed by gating for CD138<sup>+</sup>, annexin V<sup>+</sup>, and PI<sup>+</sup> cells (Fig. 7B; Supplementary Fig. S5B; Supplementary Table S4). Pretreatment of multiple myeloma cells followed by co-culture with T cells generated a significant two-fold increase in myeloma cell death ( $P \leq 0.0011$ ). Untreated multiple myeloma cells co-cultured with T cells yielded a slight increase in tumor cell death. Treatment of RPMI-8226, ARH-77, and U266 cells with



**Figure 4.**

Compound A effect on SIINFEKL-MHC-I presentation and the murine immunopeptidome. **A**, Effect of top eight hits that increased proteasomal ChT-like activity with SIINFEKL-MHC-I complex presentation on lysis of E.G7-Ova cells by the B3Z T-cell hybridoma. E.G7-Ova cells were pretreated with compounds (1 μmol/L), after which the cells were washed and co-cultured with the H-2Kb-restricted B3Z T cells genetically engineered to express a TCR that specifically recognizes the SIINFEKL-H2Kb complex. E.G7-Ova cells were co-cultured with B3Z cells at an E:T ratio of 3:1 for 24 and 48 hours. **B**, Effect of compound A on the number of peptides eluted from MHC-I (M1/42) of E.G7-ova cells. **C**, Effect of compound A on total peptide peak intensity after elution with mouse MHC-I (M1/42). **D**, Effect of compound A on E.G7-Ova presentation of SIINFEKL-MHC-I. **E**, Parallel reaction monitoring analysis of lysates spiked with the SIINFEKL peptide show that pretreatment with compound A resulted in an increase in SIINFEKL peptide copy number bound/cell by >1.5-fold. **F**, The number of peptides eluted from MHC-I (M1/42) were 8 to 9 amino acids in length, with no significant difference between treated and untreated samples. **G**, Pretreatment of E.G7-Ova cells with compound A increased the presentation of MHC-I-specific peptides by up to 50-fold. More than 450 peptides were increased by 2-fold with compound A treatment. **H**, Rank order of genes of the top 20 MHC-I-restricted peptides upregulated in cells treated with compound A. Red stars indicate peptide that has undergone posttranslational methionine oxidation. FC, fold change.

**Figure 5.**

Effect of compound A on the myeloma immunopeptidome. **A**, Effect of compound A on number of peptides eluted from MHC-I (W6/32) in RPMI-8226 cells. Cells were pretreated with compound A (1  $\mu\text{mol/L}$ ) for 48 hours, after which they were pelleted, lysed, and immunoprecipitated with human MHC-I (W6/32). Acid elution resulted in the identification of MHC-I peptide abundance in cells treated with compound A relative to untreated cells. **B**, Total peak intensity of peptides eluted from pan-MHC-I (W6/32) was increased by two-fold with compound A. **C**, Length of peptides eluted from MHC-I (W6/32). **D**, Pretreatment of RPMI-8226 cells with compound A increased the presentation of MHC-I-specific peptides up to 200-fold. More than 1,500 peptides were increased two-fold after treatment of cells with compound A. **E**, Waterfall plot representing peptides upregulated by compound A and downregulated by bortezomib treatment of RPMI-8226 cells. **F**, Effect of compound A on antigen peptide terminal residue. Greater than 80% of the top 50 peptides upregulated by compound A had a hydrophobic terminal aliphatic or aromatic residue. **G**, Genes that encode the respective MHC-I-restricted peptides upregulated and downregulated after compound A or bortezomib treatment. **H**, Rank order of genes that encode the 20 MHC-I-restricted peptides most upregulated after compound A treatment. BTZ, bortezomib; FC, fold change.

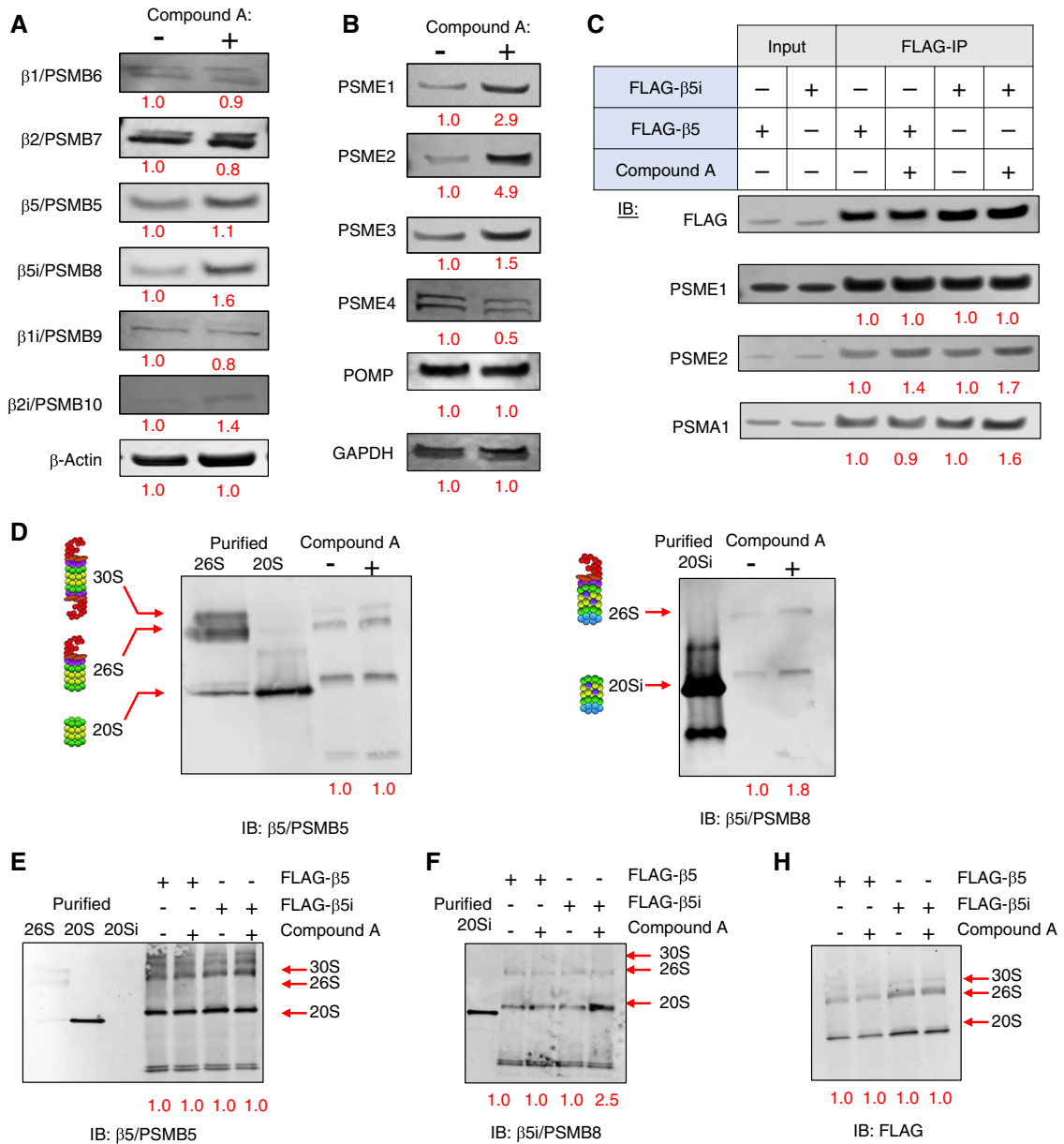


**Figure 6.**

Effect of compound A on immunoproteasome subunit β5i /PSMB8 association with the proteasome activator and immunoproteasome. **A**, Effect of compound A on proteasome and immunoproteasome catalytic subunit levels. **B**, Effect of compound A on proteasome activator subunit levels. **C**, Effect of compound A on PSME1 and PSME2 association with FLAG-tagged β5i/PSMB8 and FLAG-tagged β5/PSMB5 in cell lysates. **D**, Effect of compound A treatment on the incorporation of β5i/PSMB8 and β5/PSMB5 into endogenous 20S/26S/30S proteasomal complexes. Complexes were detected by native-PAGE and immunoblotting. **E**, **F**, and **G**, Effect of compound A on FLAG-tagged β5i/PSMB5 and FLAG-tagged β5i/PSMB8 high molecular weight proteasomal complexes in RPMI-8226 lysates. Purified 20S, 26S, and 20Si immunoproteasomes were loaded as controls for migration distance and β5i/PSMB8 or β5/PSMB5 composition. Membranes were probed with antibodies specific to β5/PSMB5 (**E**), β5i/PSMB8 (**F**), and FLAG (**G**). IB, immunoblot.

compound A alone did not induce cell death. Treatment of patient CD138<sup>+</sup> cells with compound A followed by co-culture with autologous T cells increased myeloma cell death (**Fig. 7C**). Pretreatment of patient CD138<sup>+</sup> cells with compound A without T cells or treatment with autologous T cells alone did not increase cell death. The results indicate that compound A enhanced antigen presentation to drive CTL-mediated anti-myeloma immunity. Treatment of CD8<sup>+</sup> T cells with

compound A reduced PD1 expression, without changing TIM-3, CTLA-4, or LAG-3 expression (Supplementary Fig. S5C).

**Compound A increases the anti-myeloma activity of CTLs alone and combined with ICIs**

PDL1 is overexpressed on malignant cells and binds the immunosuppressive marker PD protein-1 (PD1) to inhibit the

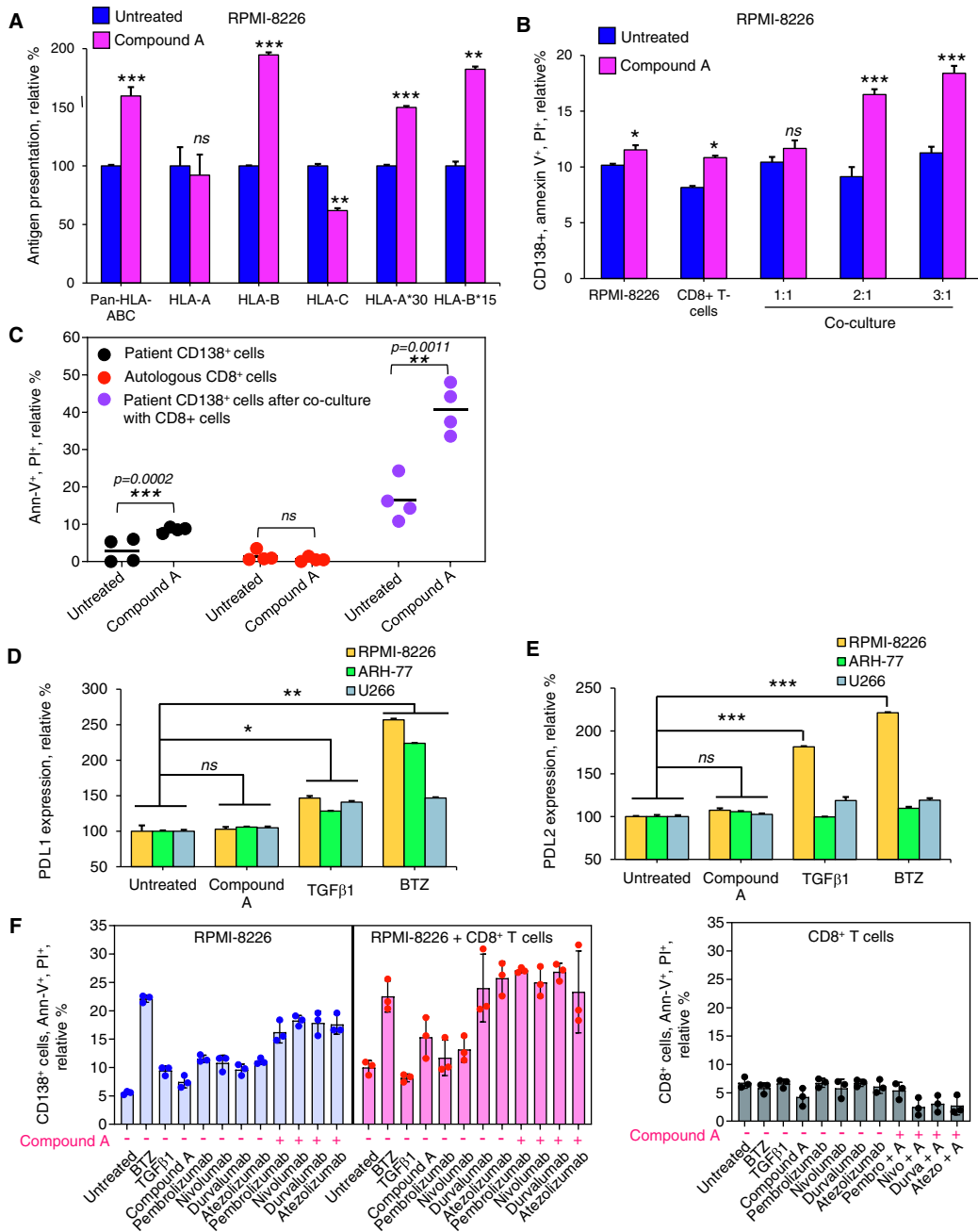


**Figure 7.**

Effect of compound A on allogenic and autologous T-cell anti-myeloma cytotoxicity. **A**, RPMI-8226 cells were treated with compound A and probed with pan-MHC-I or MHC-I subtype allele-specific antibodies, after which the samples were analyzed by flow cytometry. Pretreatment with compound A significantly increased pan-MHC-I HLA-ABC and HLA-B surface presentation in all MMCLs assayed. **B**, RPMI-8226 were pretreated with compound A for 48 hours, after which they were washed and co-cultured with healthy CD8<sup>+</sup> cytotoxic T cells for 18 hours at E:T ratios of 1:1, 2:1, and 3:1. Compound A increased CTL-mediated cytotoxicity of tumor cells, which was measured by gating for CD138<sup>+</sup>, annexin V<sup>+</sup>, and PI<sup>+</sup> cells at E:T 2:1 and 3:1. Pretreatment of MMCLs and T cells alone with compound A resulted in ~5 to 10% cell death, which was enhanced further when multiple myeloma cells were co-cultured at E:T ratios of 2:1 and 3:1. T cells alone also did not show significant cell death when pretreated with compound A. There was <5% multiple myeloma cell death detected with or without compound A treatment. Similar results were observed with CD8<sup>+</sup> T cells alone. **C**, Patient multiple myeloma CD138<sup>+</sup> cells were treated with compound A followed by co-culturing with CD8<sup>+</sup> patient-derived autologous T cells (E:T = 2:1). Cytotoxicity was measured by gating for CD138<sup>+</sup>, annexin V<sup>+</sup>, and PI<sup>+</sup> cells. **D** and **E**, Effect of compound A on PDL1 or PDL2 expression in MMCLs. **D** and **E**, Surface markers were quantitated by flow cytometry. TGFβ and BTZ were included as positive controls as they are known to upregulate PDL1/L2 expression. **F**, Effect of compound A on the viability of RPMI-8226 cells alone or combined with ICIs and CD8<sup>+</sup> T cells. Multiple myeloma and CD8<sup>+</sup> T cells were separately treated with or without compound A and the indicated agents (BTZ, TGFβ, and ICIs). Following co-culture, the relative percent of viable multiple myeloma cells was quantitated by annexin V and PI staining and flow cytometry. Assays were performed in triplicate. Ann-V, annexin V; BTZ, bortezomib.

proliferation of PD1-positive cells (44). PDL1 binding to PD1 on immune cells facilitates tumor progression by precluding CTL effector activity leading to treatment failure (45–47). Although PD1/PDL1-targeted therapies have revolutionized cancer therapy, the majority of patients are unresponsive, hyperprogressive, or develop drug resistance. Treatment of MMCLs with compound A did not effect PDL1 and PDL2 expression (Fig. 7D and E). We next queried whether the ICIs, which function by blocking checkpoint proteins from binding with their partner proteins, enhanced the cytotoxic effect of T cells on compound A-treated multiple myeloma cells. Treatment of three different MMCLs with compound A alone, each ICI alone, or compound A combined with an ICI yielded only ~7% to 15% apoptosis of tumor cells (Fig. 7F; Supplementary Fig. S6). Treatment of tumor cells with allogeneic T cells also generated only ~5% apoptotic in myeloma cells. However, treatment of the multiple myeloma cells with compound A significantly increased T-cell anti-myeloma activity by ~20% to 30% when combined with pembrolizumab, nivolumab, durvalumab, or atezolizumab.

#### Pretreatment of E.G7-Ova-GFP-Luc cells with compound A reduces tumor growth *in vivo*

We next determined the effect of compound A on the growth of E.G7-Ova-GFP-Luc cells injected into OT-1 mice (Supplementary Fig. S7A–S7G). OT-1 mice contain a transgenic TCR that recognizes Ova residues 257 to 264 in the context of the H2K<sup>b</sup> class-I molecule interaction. This results in MHC-I-restricted, Ova-specific, CD8<sup>+</sup> T cells (OT-I cells). E.G7-Ova-GFP-Luc cells were pretreated with vehicle or compound A and injected into mice. TBW of mice injected with compound A-treated E.G7-Ova cells was similar to that of mice injected with vehicle-treated cells. Also, we did not detect an effect of the compound A-treated cells on appetite, gait, skin turgor, or musculoskeletal or neurologic systems (Supplementary Fig. S7D). Tumor growth was monitored by quantitating the BLI ROI represented by total flux (p/s). Results indicated that *ex vivo* pretreatment with compound A reduced the *in vivo* growth of E.G7-Ova-GFP-Luc cells compared with the growth of E.G7-Ova-GFP-Luc cells treated with vehicle (Supplementary Fig. S7E and S7F). Pretreatment of E.G7-Ova-GFP-Luc cells with compound A also extended mouse survival compared with that of mice injected with E.G7-Ova-GFP-Luc cells treated with vehicle alone (Supplementary Fig. S7G).

#### *In vivo* administration of compound A reduces the growth of myeloma xenotransplants

We assessed the *in vivo* tolerability and effect of compound A on myeloma xenotransplants in NOD/SCID gamma mice (Supplementary Fig. S8A–S8E). Mice were injected with MM1.S-Luc cells and randomized into four groups (seven mice/group) that were treated with either vehicle, compound A, healthy T cells, or both compound A and T cells. Results indicated that compound A was well-tolerated *in vivo* and did not induce appreciable changes in TBW, appetite, gait, skin turgor, or neurologic or musculoskeletal systems (Supplementary Fig. S8C). Caliper measurements indicated that co-treatment with compound A and T cells significantly reduced tumor volume compared with the other treatment groups (Supplementary Fig. S8D). BLI measurements in mice treated with both compound A and T cells *in vivo* were reduced relative to the other groups (Supplementary Fig. S8E). Taken together, the results suggest *in vivo* tolerability and anti-myeloma activity of compound A and support the translational relevance of our study. Lastly, we queried whether compound A impacted the antitumor activity of bortezomib. Proteasome inhibitors are key in the treatment of

patients with newly diagnosed or Relapsed and/or Refractory Multiple Myeloma. Treatment of MMCLs or E.G7-Ova cells with bortezomib alone or combined with compound A yielded significant cell death (Supplementary Fig. S9A–S7D). Compound A did not increase or counteract the anti-myeloma activity of bortezomib.

## Discussion

Antigen presentation is central for the adaptive immune system to distinguish self from non-self and the detection of malignant cells. Presentation of immunogenic peptides, for example, non-mutated cancer-associated antigens and NeoAgs, on malignant cells facilitates their recognition and destruction by CD8<sup>+</sup> T cells. A central challenge is the magnitude of mutations generated within cancer-associated genes that are translated into tumor-specific antigens to exponentially expand the human immunopeptidome. Immunologic discernment takes place at the cellular level, and the immune system mounts cytotoxic responses against immunogenic antigens to prevent tumor development or promote tumor regression. These observations incriminate deregulation of the APM as a central mechanism of immune evasion that cancers have developed to subvert adaptive immunity. Constitutive and immunoproteasomes have evolved through gene duplication to discriminate self from non-self and are central to the detection of cancer cells by effectors of adaptive immunity (48, 49). Immunoproteasome activation represents a transformative approach to boost the antitumor activity of endogenous and engineered T-cell immunotherapies.

The presented peptide repertoire, the class-I immunopeptidome, is generated from each cell's transcriptome in a biased manner to avoid overrepresenting highly abundant translation products. Currently, the immunopeptidome can be defined by MS methods. Our MS/proteomic studies indicate that compound A treatment of multiple myeloma cells increased the presentation of numerous peptide epitopes as a consequence of increased processing of the same protein. These findings are consistent with the role of the proteasome activator PA28 $\alpha/\beta$  in immunoproteasome activity. In addition, we also observed that compound A treatment increased the representation of Tyr or Phe as the terminal amino acid of the most upregulated peptides to suggest that compound A directly modulates the immunoproteasomal cleavage pattern. IFN $\gamma$  also alters the immunopeptidome, binds to IFN $\gamma$  receptors, activates JAK/STAT signaling, and leads to the expression of IFN-response factor transcription factors and a multitude of IFN $\gamma$ -regulated genes that elicit major changes in the transcriptome and proteome (50). Proteins involved in the processing and presentation of antigens on HLA-I molecules are particularly upregulated by IFN $\gamma$ , including the immunoproteasome catalytic subunits *PSMB8*, *PSMB9*, and *PSMB10*, and peptidases which can trim peptides prior to loading onto HLAs, for example, LAP3 (51), THOP1 (52), ERAP1 (53), and ERAP2 (54). The peptide transporters TAP1 and TAP2, which shuttle peptides into the endoplasmic reticulum where HLA loading occurs, are also upregulated as well as HLA expression (55). In contrast to compound A, IFN $\gamma$  promotes the expression of PDL1 and IDO1, immunosuppressive molecules that suppress T-cell activity. The direct effect of compound A on immunoproteasomes without an effect on other components of the APM and PDL1/PDL2 may offer advantages and reduce any unwanted on-target/off-tumor effects.

Emerging T-cell-based therapies, for example, CAR T cells, TCR-engineered cells, and adoptive T-cell transfer, have focused on the presentation of cancer-associated antigens. Although the

mechanisms of action behind these therapies vary tremendously, the core component is inducing the ability of T cells to kill cancer cells after their TCRs recognize the appropriate MHC-complexed peptides. Identification and prediction of tumor-specific NeoAgs have been made possible by the advanced development of proteomic methods, next-generation sequencing, and bioinformatic technologies. Compared with TAAgs, the highly immunogenic and tumor-specific NeoAgs provide emerging targets to personalize cancer immunotherapies and serve as prospective predictors for tumor survival, prognosis, and response to immune checkpoint blockade. Treatment of multiple myeloma cells with compound A increased the level of non-mutated public antigens as well as private NeoAgs that result from non-synonymous somatic mutations in cancer cells (56, 57). Public antigens can be shared by multiple cancers but can also be expressed on normal tissues, whereas NeoAgs are tumor-specific and generally also patient-specific. Targeting NeoAgs enables tumor destruction without undue damage to vital healthy tissues.

CD8<sup>+</sup> T cells, especially their capacity for antigen-directed cytotoxicity, have become a central focus for engaging the immune system in the fight against cancer. Adoptive T-cell therapy, in which autologous or allogenic T cells are infused into patients with cancer, has shown considerable promise. Innovative approaches to promote T-cell activity and proliferation may allow for a greater palette of treatments to be developed. A limitation to the development of CAR T-cell therapies is the requirement for a distinct tissue-restricted target antigen on the tumor cell surface. Toxicities can arise from CAR T-cell therapy and affect many different organ systems with a range of severities. Agents that increase immunoproteasome activity to enhance MHC-I antigen presentation offer potential as a rapid, cost-effective, off-the-shelf approach to enhance the activity of allogenic and autologous T-cell therapy and to directly target tumor cells. Although little is known about the factors that modulate the threshold for antigen recognition, insufficient reactivity against cells with low antigen density has emerged as an important cause of CAR T-cell resistance (58). Importantly, optimal endogenous T-cell and CAR T-cell efficacy is dependent on antigen density, and immunoproteasome activation increases the density of many antigens. Biologic signaling systems exhibit vast, nonlinear responses to T cells that may be manipulated to better discriminate between cancer cells and healthy tissues (59). The ability to achieve ultrasensitive antigen-density discrimination provides a critical tool for widening the therapeutic window of endogenous and engineered T cells against cancers, in which many TAAgs are overexpressed but not absolutely tumor-specific (60).

In virtually all cell types, multiple proteasome forms govern myriad essential processes. Proteasome activity is regulated by endogenous inhibitory proteins, and incorporation of the 20S proteasome into the ubiquitin conjugate-degrading 26S complex clearly alters the catalytic properties (61). Similarly, at least three endogenous proteasome activators—PA28, PA200, and PA700—are relatively abundant in human cells and strongly support a fundamental biologic role for proteasomal activators under physiologic and pathologic conditions (62). Pharmacologic modulation of proteasomal activity represents a proven and emerging strategy to treat human diseases. The FDA-approved proteasome inhibitors bortezomib and carfilzomib selectively and effectively target multiple myeloma cells, and carfilzomib is the first and only multiple myeloma treatment that extends overall survival in the relapsed setting over the current standard of care (63, 64). Likewise, immunoproteasome-specific inhibitors

are in development to treat autoimmune diseases, inflammatory processes, and allogeneic organ transplant rejection (33). Drug-like proteasome activators and agonists, in contrast to proteasome inhibitors, are only beginning to emerge to treat numerous proteinopathies, age-related dysfunction in proteostasis, and Alzheimer's disease (65, 66). We envision the future development of immunoproteasome-specific activators that increase NeoAg presentation to boost T-cell-driven tumor lysis.

The ability of cells to maintain proteostasis and a healthy proteome gradually declines during aging (67). Aging is paralleled by a decline in proteasome activity in multicellular organisms and leads to a number of age-related diseases through mechanisms that remain poorly understood. In addition, autosomal recessive homozygous or compound heterozygous loss-of-function mutations in *PSMB8* cause a syndrome that has historically been referred to as joint contractures, muscle atrophy, microcytic anemia, and panniculitis-induced childhood-onset lipodystrophy syndrome, Nakajo–Nishimura syndrome, or chronic atypical neutrophilic dermatosis and constitute a spectrum of proteasome-associated autoinflammatory syndromes (ref. 68). Bio-medical implications of immunoproteasome activators may be significant to overcome deficiencies in immunoproteasome activity as seen in proteasome-associated autoinflammatory syndromes, as well as modulate antitumor immune responses, autoimmune and neurodegenerative diseases, and aging.

## Authors' Disclosures

E. Malek reports being on the advisory board for Bristol Myers Squibb, Janssen, and Amgen; research funding from MedPacto Inc.; and being a speaker for Bristol Myers Squibb and Janssen. D.J. Adams reports personal fees and other support from Convelo Therapeutics outside the submitted work. J.J. Driscoll reports a patent for UH Ventures pending. No disclosures were reported by the other authors.

## Authors' Contributions

**P.S. Rana:** Conceptualization, data curation, validation, investigation, methodology, writing—original draft, writing—review and editing. **J.J. Ignatz-Hoover:** Data curation, formal analysis, validation, investigation, methodology, project administration, writing—review and editing. **C. Guo:** Software, formal analysis, methodology, writing—review and editing. **A.L. Mosley:** Formal analysis, investigation, visualization, methodology, writing—review and editing. **E. Malek:** Formal analysis, investigation. **Y. Fedorov:** Formal analysis, validation, investigation, methodology. **D.J. Adams:** Formal analysis, validation, investigation, methodology. **J.J. Driscoll:** Conceptualization, resources, formal analysis, supervision, funding acquisition, validation, investigation, visualization, methodology, writing—original draft, project administration, writing—review and editing.

## Acknowledgments

This research was supported by NIH R01 (5R01AI139141), the UH Seidman Cancer Center, the Vinney Foundation, and the Case Comprehensive Cancer Center (to J.J. Driscoll). This research was supported by the Translational Research Shared Resources of the Case Comprehensive Cancer Center (P30 CA#43703). The authors state that the Life Technologies Attune NxT Flow Cytometer was acquired through an NIH Shared Instrumentation Grant, and, as such, we are required by NIH Regulations to specifically cite the assistance of the Case Comprehensive Cancer Center Cytometry & Microscopy Shared Resource and NIH Grant S10-NIH OD021559.

## Note

Supplementary data for this article are available at Molecular Cancer Therapeutics Online (<http://mct.aacrjournals.org/>).

Received December 29, 2023; revised April 30, 2024; accepted August 16, 2024; published first August 30, 2024.

## References

- Yang K, Halima A, Chan TA. Antigen presentation in cancer—mechanisms and clinical implications for immunotherapy. *Nat Rev Clin Oncol* 2023;20:604–23.
- Waldman AD, Fritz JM, Lenardo MJ. A guide to cancer immunotherapy: from T cell basic science to clinical practice. *Nat Rev Immunol* 2020;20:651–68.
- Sharma P, Hu-Lieskovan S, Wargo JA, Ribas A. Primary, adaptive, and acquired resistance to cancer immunotherapy. *Cell* 2017;168:707–23.
- Sijts EJ, Kloetzel PM. The role of the proteasome in the generation of MHC class I ligands and immune responses. *Cell Mol Life Sci* 2011;68:1491–502.
- Desjardins M. Antigen cross-presentation: proteasome location, location, location. *EMBO J* 2019;38:e102799.
- Brown MG, Driscoll JJ, Monaco JJ. Structural and serological similarity of MHC-linked LMP and proteasome (multicatalytic proteinase) complexes. *Nature* 1991;353:355–7.
- Yewdell JW. Immunoproteasomes: regulating the regulator. *Proc Natl Acad Sci USA* 2005;102:9089–90.
- Ferrington DA, Gregerson DS. Immunoproteasomes: structure, function, and antigen presentation. *Prog Mol Biol Transl Sci* 2012;109:75–112.
- Jhunjhunwala S, Hammer C, Delamarre L. Antigen presentation in cancer: insights into tumour immunogenicity and immune evasion. *Nat Rev Cancer* 2021;21:298–312.
- Zamora AE, Crawford JC, Thomas PG. Hitting the target: how T cells detect and eliminate tumors. *J Immunol* 2018;200:392–9.
- Leko V, Rosenberg SA. Identifying and targeting human tumor antigens for T cell-based immunotherapy of solid tumors. *Cancer Cell* 2020;38:454–72.
- Lee MY, Jeon JW, Sievers C, Allen CT. Antigen processing and presentation in cancer immunotherapy. *J Immunother Cancer* 2020;8:e001111.
- Dhatchinamoorthy K, Colbert JD, Rock KL. Cancer immune evasion through loss of MHC class I antigen presentation. *Front Immunol* 2021;12:636568.
- Carretero FJ, Del Campo AB, Flores-Martín JF, Mendez R, García-López C, Cozar JM, et al. Frequent HLA class I alterations in human prostate cancer: molecular mechanisms and clinical relevance. *Cancer Immunol Immunother* 2016;65:47–59.
- Cabrera T, Maleno I, Lopez-Nevot MA, Redondo M, Fernandez MA, Collado A, et al. High frequency of HLA-B44 allelic losses in human solid tumors. *Hum Immunol* 2003;64:941–50.
- McGranahan N, Rosenthal R, Hiley CT, Rowan AJ, Watkins TBK, Wilson GA, et al. Allele-specific HLA loss and immune escape in lung cancer evolution. *Cell* 2017;171:1259–71.e11.
- Mumphrey MB, Hossaini N, Parolia A, Geng J, Zou W, Raghavan M, et al. Distinct mutational processes shape selection of MHC class I and class II mutations across primary and metastatic tumors. *Cell Rep* 2023;42:112965.
- Kalaora S, Lee JS, Barnea E, Levy R, Greenberg P, Alon M, et al. Immunoproteasome expression is associated with better prognosis and response to checkpoint therapies in melanoma. *Nat Commun* 2020;11:896.
- Balasubramanian A, John T, Asselin-Labat ML. Regulation of the antigen presentation machinery in cancer and its implication for immune surveillance. *Biochem Soc Trans* 2022;50:825–37.
- Tripathi SC, Peters HL, Taguchi A, Katayama H, Wang H, Momin A, et al. Immunoproteasome deficiency is a feature of non-small cell lung cancer with a mesenchymal phenotype and is associated with a poor outcome. *Proc Natl Acad Sci USA* 2016;113:E1555–64.
- Spits M, Neefjes J. Immunoproteasomes and immunotherapy—a smoking gun for lung cancer? *J Thorac Dis* 2016;8:E558–63.
- Fresneda PM, Bleda JA, Sanz MA, Molina P. Aza-Wittig reaction, carbodiimide-mediated ring closure, and enol-induced ring interconversion: a domino process for the synthesis of 4-methylene-4H-3, 1-benzoxazines. *Synlett* 2007;2007:1541–4.
- Butler KV, Kalin J, Brochier C, Vistoli G, Langley B, Kozikowski AP. Rational design and simple chemistry yield a superior, neuroprotective HDAC6 inhibitor, tubastatin A. *J Am Chem Soc* 2010;132:10842–6.
- Jochems J, Boulden J, Lee BG, Blenny JA, Jarpe M, Mazitschek R, et al. Antidepressant-like properties of novel HDAC6-selective inhibitors with improved brain bioavailability. *Neuropsychopharmacology* 2014;39:389–400.
- Santo L, Hideshima T, Kung AL, Tseng J-C, Tamang D, Yang M, et al. Pre-clinical activity, pharmacodynamic, and pharmacokinetic properties of a selective HDAC6 inhibitor, ACY-1215, in combination with bortezomib in multiple myeloma. *Blood* 2012;119:2579–89.
- Bergman JA, Woan K, Perez-Villarreal P, Villagra A, Sotomayor EM, Kozikowski AP. Selective histone deacetylase 6 inhibitors bearing substituted urea linkers inhibit melanoma cell growth. *J Med Chem* 2012;55:9891–9.
- Scudiero DA, Shoemaker RH, Paull KD, Monks A, Tierney S, Nofziger TH, et al. Evaluation of a soluble tetrazolium/formazan assay for cell growth and drug sensitivity in culture using human and other tumor cell lines. *Cancer Res* 1988;48:4827–33.
- Nyayapathy S, Jones R, Ford M, Doty M, Rumble JM. Abstract 2996: CT26 neoantigen presentation and immunogenicity. *Cancer Res* 2023;83:2996.
- Roelofs J, Supphiah A, Waite KA, Park S. Native gel approaches in studying proteasome assembly and chaperones. *Methods Mol Biol* 2018;1844:237–60.
- Rana PS, Ignatz-Hoover J, Driscoll JJ. Abstract 6235: discovery of novel HDAC6 inhibitors that enhance proteasomal activity to boost antigen presentation and trigger anti-myeloma T-cell immunity. *Cancer Res* 2023;83:6235.
- Bard JAM, Goodall EA, Greene ER, Jonsson E, Dong KC, Martin A. Structure and function of the 26S proteasome. *Annu Rev Biochem* 2018;87:697–724.
- Miller Z, Ao L, Kim KB, Lee W. Inhibitors of the immunoproteasome: current status and future directions. *Curr Pharm Des* 2013;19:4140–51.
- Xi J, Zhuang R, Kong L, He R, Zhu H, Zhang J. Immunoproteasome-selective inhibitors: an overview of recent developments as potential drugs for hematologic malignancies and autoimmune diseases. *Eur J Med Chem* 2019;182:111646.
- Peck Justice SA, Barron MP, Qi GD, Wijeratne HRS, Victorino JF, Simpson ER, et al. Mutant thermal proteome profiling for characterization of missense protein variants and their associated phenotypes within the proteome. *J Biol Chem* 2020;295:16219–38.
- Peck Justice SA, McCracken NA, Victorino JF, Qi GD, Wijeratne AB, Mosley AL. Boosting detection of low-abundance proteins in thermal proteome profiling experiments by addition of an isobaric trigger channel to TMT multiplexes. *Anal Chem* 2021;93:7000–10.
- Moore MW, Carbone FR, Bevan MJ. Introduction of soluble protein into the class I pathway of antigen processing and presentation. *Cell* 1988;54:777–85.
- Harms JS, Khan M, Hall C, Splitter GA, Homan EJ, Bremel RD, et al. Brucella peptide cross-reactive major histocompatibility complex class I presentation activates SIINFEKL-specific T cell receptor-expressing T cells. *Infect Immun* 2018;86:e00281–18.
- Smith CC, Selitsky SR, Chai S, Armistead PM, Vincent BG, Serody JS. Alternative tumour-specific antigens. *Nat Rev Cancer* 2019;19:465–78.
- Yarchoan M, Johnson BA III, Lutz ER, Laheru DA, Jaffee EM. Targeting neoantigens to augment antitumour immunity. *Nat Rev Cancer* 2017;17:569.
- Karoulia Z, Gavathiotis E, Poulidakos PI. New perspectives for targeting RAF kinase in human cancer. *Nat Rev Cancer* 2017;17:676–91.
- Bose M, Mukherjee P. Potential of anti-MUC1 antibodies as a targeted therapy for gastrointestinal cancers. *Vaccines (Basel)* 2020;8:659.
- Pulanco MC, Madsen AT, Tanwar A, Corrigan DT, Zang X. Recent advancements in the B7/CD28 immune checkpoint families: new biology and clinical therapeutic strategies. *Cell Mol Immunol* 2023;20:694–713.
- Sherr CJ, Beach D, Shapiro GI. Targeting CDK4 and CDK6: from discovery to therapy. *Cancer Discov* 2016;6:353–67.
- Liu J, Chen Z, Li Y, Zhao W, Wu J, Zhang Z. PD-1/PD-L1 checkpoint inhibitors in tumor immunotherapy. *Front Pharmacol* 2021;12:731798.
- Greten TF, Villanueva A, Korangy F, Ruf B, Yarchoan M, Ma L, et al. Biomarkers for immunotherapy of hepatocellular carcinoma. *Nat Rev Clin Oncol* 2023;20:780–98.
- Hudson K, Cross N, Jordan-Mahy N, Leyland R. The extrinsic and intrinsic roles of PD-L1 and its receptor PD-1: implications for immunotherapy treatment. *Front Immunol* 2020;11:568931.
- Murata S, Takahama Y, Kasahara M, Tanaka K. The immunoproteasome and thymoproteasome: functions, evolution and human disease. *Nat Immunol* 2018;19:923–31.
- Thibaudeau TA, Smith DM. A practical review of proteasome pharmacology. *Pharmacol Rev* 2019;71:170–97.
- Miller Z, Lee W, Kim KB. The immunoproteasome as a therapeutic target for hematological malignancies. *Curr Cancer Drug Targets* 2014;14:537–48.
- Hewat A, Yu L, Barber L, Choudhary J, Bassani-Sternberg M, Gerlinger M. Multifactorial remodeling of the cancer immunopeptidome by IFN $\gamma$ . *Cancer Res Commun* 2023;3:2345–57.

51. Beninga J, Rock KL, Goldberg AL. Interferon- $\gamma$  can stimulate post-proteasomal trimming of the N terminus of an antigenic peptide by inducing leucine aminopeptidase. *J Biol Chem* 1998;273:18734–42.
52. Saric T, Beninga J, Graef CI, Akopian TN, Rock KL, Goldberg AL. Major histocompatibility complex class I-presented antigenic peptides are degraded in cytosolic extracts primarily by thimet oligopeptidase. *J Biol Chem* 2001;276:36474–81.
53. Saric T, Chang S-C, Hattori A, York IA, Markant S, Rock KL, et al. An IFN- $\gamma$ -induced aminopeptidase in the ER, ERAP1, trims precursors to MHC class I-presented peptides. *Nat Immunol* 2002;3:1169–76.
54. Saveanu L, Carroll O, Lindo V, Del Val M, Lopez D, Lepelletier Y, et al. Concerted peptide trimming by human ERAP1 and ERAP2 aminopeptidase complexes in the endoplasmic reticulum. *Nat Immunol* 2005;6:689–97.
55. Zhou F. Molecular mechanisms of IFN- $\gamma$  to up-regulate MHC class I antigen processing and presentation. *Int Rev Immunol* 2009;28:239–60.
56. Xie N, Shen G, Gao W, Huang Z, Huang C, Fu L. Neoantigens: promising targets for cancer therapy. *Sig Transduct Target Ther* 2023;8:9.
57. Pearlman AH, Hwang MS, Konig MF, Hsiue EH-C, Douglass J, DiNapoli SR, et al. Targeting public neoantigens for cancer immunotherapy. *Nat Cancer* 2021;2:487–97.
58. Majzner RG, Rietberg SP, Sotillo E, Dong R, Vachharajani VT, Labanieh L, et al. Tuning the antigen density requirement for CAR T-cell activity. *Cancer Discov* 2020;10:702–23.
59. Suresh S, O'Donnell KA. Translational control of immune evasion in cancer. *Trends Cancer* 2021;7:580–2.
60. Hernandez-Lopez RA, Yu W, Cabral KA, Creasey OA, Lopez Pazmino MDP, Tonai Y, et al. T cell circuits that sense antigen density with an ultrasensitive threshold. *Science* 2021;371:1166–71.
61. Driscoll JJ, Frydman J, Goldberg AL. An ATP-stabilized inhibitor of the proteasome is a component of the 1500-kDa ubiquitin conjugate-degrading complex. *Proc Natl Acad Sci U S A* 1992;89:4986–90.
62. Stadtmueller BM, Hill CP. Proteasome activators. *Mol Cell* 2011;41:8–19.
63. Richardson PG, Sonneveld P, Schuster MW, Irwin D, Stadtmauer EA, Facon T, et al. Bortezomib or high-dose dexamethasone for relapsed multiple myeloma. *N Engl J Med* 2005;352:2487–98.
64. Dimopoulos MA, Goldschmidt H, Niesvizky R, Joshua D, Chng WJ, Oriol A, et al. Carfilzomib or bortezomib in relapsed or refractory multiple myeloma (ENDEAVOR): an interim overall survival analysis of an open-label, randomised, phase 3 trial. *Lancet Oncol* 2017;18:1327–37.
65. Njomen E, Tepe JJ. Proteasome activation as a new therapeutic approach to target proteotoxic disorders. *J Med Chem* 2019;62:6469–81.
66. Chocron ES, Munkácsy E, Kim HS, Karpowicz P, Jiang N, Van Skike CE, et al. Genetic and pharmacologic proteasome augmentation ameliorates Alzheimer's-like pathology in mouse and fly APP overexpression models. *Sci Adv* 2022;8:eabk2252.
67. Rana PS, Ignatz-Hoover JJ, Driscoll JJ. Targeting proteasomes and the MHC class I antigen presentation machinery to treat cancer, infections and age-related diseases. *Cancers (Basel)* 2023;15:5632.
68. Brehm A, Liu Y, Sheikh A, Marrero B, Omoyinmi E, Zhou Q, et al. Additive loss-of-function proteasome subunit mutations in CANDLE/PRAAS patients promote type I IFN production. *J Clin Invest* 2015;125:4196–211.